International Journal of Mechanical Sciences 320 (2026) 111619

Contents lists available at ScienceDirect

International Journal of Mechanical Sciences

journal homepage: www.elsevier.com/locate/ijmecsci

A novel tire-pavement related parameter for improved rolling resistance predictions

W.A.A.S. Premarathna [a], Kumar Anupam [a,*], M. Moenielal [b], Thijs Wensveen [c], Cor Kasbergen [a], Sandra M.J.G. Erkens [a]

[a] Section of Pavement Engineering, Faculty of Civil Engineering and Geosciences, Delft University of Technology, Stevinweg 1, 2628 CN, Delft, the Netherlands
[b] Section of Buildings, Materials and Structures, TNO, Molengraaffsingel 8, 2628 JD Delft, the Netherlands
[c] Section of Intelligent Imaging, TNO, Oude Waalsdorperweg, Den Haag, the Netherlands

ARTICLE INFO

Keywords:
Machine learning
Finite element method
Tire industries
Tire-pavement interaction
Tire penetration level
Rolling resistance

ABSTRACT

Accurate prediction of rolling resistance (RR) is essential for improving vehicle fuel efficiency and supporting policymakers in making sustainable environmental decisions. This study introduces a novel framework that integrates both data-driven and physics-based approaches to enhance RR prediction by incorporating tire-penetration level indicator, the Delta (δ) parameter. The research investigates the relationships between RR, the δ parameter, and texture properties to refine predictive modelling. A portable device was built to measure the in-field δ parameter using tire-pavement interaction. Machine learning (ML) techniques, including multiple linear regression (MLR), random forest regressor (RFR), artificial neural networks (ANN) and finite element method-based (FEM) tire-pavement interaction models were employed to develop and validate the framework. Findings from the FEM tire-pavement interaction model confirmed the reliability of the δ parameter. Exploratory data analysis (EDA) highlighted the strong correlation between texture metrices such as MPD, ETD, and RMS, reinforcing the δ parameter's role in tire-pavement interactions. Comparative analysis of different pavement surfaces revealed that worn surfaces contribute to higher δ parameter values and increased RR. The improvement resulting from the inclusion of the δ parameter is particularly evident in the ANN and RF models, confirming nonlinear interaction effects between tire penetration and surface texture. It was also observed that the obtained RR data follow a non-normal distribution, which most of the previous studies did not consider. A deeper statistical insight showed that the δ parameter has a significant impact on RRC prediction. The primary contribution of this study lies in demonstrating the feasibility of integrating a physics-based tire-pavement interaction parameter into ML models for rolling resistance prediction, thereby bridging mechanistic modelling and machine learning within pavement engineering.

1. Introduction

A deeper understanding of tire-pavement interaction is crucial in advancing pavement design and tire manufacturing processes [1–3]. Considering the huge demand for AI-based self-driving automation systems, key performance metrics such as vehicle handling, energy efficiency, safety, and noise levels have become of paramount interest to scientists [3,–,5]. Moreover, the enhancements of key performance metrics are eventually essential for better alignment with sustainability goals [6]. Researchers [1,7–10] have extensively analysed phenomena such as skid resistance, rolling resistance, and noise generation using tire-pavement interaction mechanisms. However, to the best of the authors' knowledge rolling resistance has not been extensively addressed. Therefore, the focus of this research is on rolling resistance, which directly influences vehicle fuel efficiency [4,6,7,10]. Due to economic and environmental sustainability goals, the rolling resistance has become a key concern for both the tire and pavement industries [11–14]. Researchers [10,13,15–18] have concluded that accurate measurement of rolling resistance is difficult because it is affected by various tire and pavement related parameters. Therefore, in order to solve these complexities different methodologies have been proposed [13,19–21]. The methodologies are ranging from laboratory experiments under control conditions to empirical/analytical-based prediction models [13,19,20,22–24].

* Corresponding author at: TUDelft, the Netherlands.
E-mail address: k.anupam@tudelft.nl (K. Anupam).

https://doi.org/10.1016/j.ijmecsci.2026.111619
Received 17 September 2025; Received in revised form 5 March 2026; Accepted 10 April 2026
Available online 14 April 2026

Commonly used rolling resistance prediction models are solely based on texture parameters such as Mean Profile Depth (MPD), Root Mean Square (RMS), International Roughness Index (IRI) and Skewness [10,25–27]. However, these models have been reported to mostly result in poor accuracy and a lack of transferability [15,24]. The predictions of statistical models with reasonable correlation are restricted to specific pavement types or limited testing and operating conditions [28–30]. Hence, they provide limited capacity to effectively account for the various tire treads interacting with different pavement textures [10,15]. Also, these models neglected the role of combined influence of tire and pavement characteristics on rolling resistance [19,31]. Therefore, existing models fail to capture the complex relationship between tire and pavement interaction with surrounding conditions in the context of rolling resistance [13].

Considering the above limitations, researchers in current days tried to better understand the interaction between rolling resistance and pavement texture by utilizing computational and numerical modeling techniques [13,19,31]. However, researcher reported that such frameworks required high computational power and time to generate results [32]. Moreover, validation/verification of the numerical-based models are also challenging. The complexity of tire-pavement interaction models and the lack of available facilities make the accurate prediction of rolling resistance challenging. Therefore, the use of numerical modeling-based techniques is limited, and not all simulations could be conducted.

With respect to the computational difficulties as highlighted above, researchers in parallel tried to obtain the complex interaction behavior of tire and pavement by establishing different source of parameters. These parameters often depend on both the tire characteristics, pavement characteristics, surrounding conditions and tire properties, etc. One of the key parameters as proposed by researchers is the depth or volume of tire penetration into pavement texture [15,33–38]. The parameters related to tire penetration would be able to calculate the tire penetration in relation to surface morphology and help better prediction of rolling resistance [10,15]. The past studies have only provided a theoretical framework to calculate tire penetration depth or volume.

Hence, a parameter called the “Delta parameter (δ)” is newly introduced in this study as one of the physics-based parameters, which is related to the tire penetration depth and surface texture. The δ parameter is defined with reference to the average tire penetration depth within the tire contact patch with respect to surface morphology. More explanations of the parameter can be found in subsequent sections in this paper. To the best of the authors' knowledge, researchers have not yet attempted to incorporate the mentioned physics-based parameters into the calculation of rolling resistance.

The acquisition of tire penetration data is challenging because there are no standardized methods for measuring rubber penetration depth/volume to ensure consistency and comparability across different studies and pavement types. Ejsmont and Sommer [39] presented an approach to predicting tire penetration volume using tire rubber imprints and 3D digital texture profilometer. However, access to the measurement equipment is limited due to its availability and cost. To mitigate these drawbacks and accurately quantify the δ parameter, advancements in computer vision techniques can be utilized in combination with a smartphone. Computer vision systems can be automated to provide rapid and consistent measurements [40,41–44]. This is especially crucial when measuring factors influencing rolling resistance, where accuracy and non-contact measurements are essential under low cost.

Possible approach to improve the prediction accuracy of rolling resistance is to develop a combined framework of both data-driven and physics-driven approaches. The framework integrates the parameters governing physics-based parameters such as δ parameter with machine learning (ML) and computer vision techniques. ML approaches can capture complex, nonlinear relationships between tire and pavement characteristics [45–53]. Which offers a pathway to overcome the limitations of the traditional prediction approaches. It is expected that the models can better represent the tire pavement interaction by explicitly including δ parameter as one of the key features. However, to the best of the authors' knowledge, there is no studies that have been conducted combining both data-driven and physics-driven methods to predict the rolling resistance effectively and accurately. Hence, this study will be a research effort to scientifically estimate and predict the rolling resistance accurately by using a combination of both data-driven and physics-driven approaches while incorporating δ parameter.

The paper is organized to highlight the improvement in prediction accuracy of rolling resistance in relation to texture properties and δ parameter using a multi-method approach. The study begins by presenting a brief overview of tire penetration depth (SubSection 1.1), thereby establishing a research framework that defines the aim and scope of the research (SubSection 1.2). SubSection 1.3 provides innovative aspect of the research. Section 2 outlines the methodological approach, detailing the proposed framework and the procedure adopted for the measurement of the δ parameter. This is followed by the development and validation of numerical models for measuring the δ parameter (Section 3). The findings from these sections are analysed and interpreted in the results and discussion section (Section 4). Finally, Section 5 summarizes the conclusions and outlines potential directions for future research.

1.1. Investigation of tire penetration depth

The tire penetration level phenomenon is typically defined as the level of depth or volume intrusion of the tire tread into pavement cavities in relation to surface morphology [15,37]. As shown in Fig. 1.1, tire only partially covers a certain area of the pavement texture when it rolls over a pavement surface [15]. On pavement texture perspective, when sliding the rubber of the tire at low velocities on the surface texture, the rubber undergoes deformation in a way that perfectly conforms to the short-wavelength surface roughness profile of the substrate. This perfect contact happens due to adhesion to the substrate [54,55]. In such situations under typical conditions with the pressure applied in the contact area, the tire rubber contacts with only 5% of the pavement surface [56,57]. In contrast, at longer length scales, the contact includes the most prominent surface irregularities of the pavement. In this contact region, the local pressure is significant enough to compress the rubber material into numerous smaller-sized cavities [55,56]. Considering the above facts, the readings of the tire penetration data would change depending on the particular length scale of the selected pavement profile. Such variation in penetration levels generates fluctuating forces on the rubber surface, resulting in energy dissipation through the internal friction of the rubber. Additionally, this deformation frequently alters the magnitude of hysteresis forces, which directly contribute to the accumulation of rolling resistance [17,56].

The magnitude of hysteresis forces is notably affected by the sharpness of the texture summits, the type of pavement, and the hardness of the rubber [15]. The variations occur due to changes in summits because the contact interactions between the sharp summits (or positive texture) and the smooth summits (or negative texture) result in distinct responses from the tire rubber during the penetration process [15]. Moreover, under identical loading and surface conditions, a tire tread composed of hard rubber exhibits lower penetration into surface cavities on the pavement compared to a tread with a smoother rubber composition [15]. The type of pavement significantly changes the true contact area between the tire and the pavement and thereby influencing the level of tire penetration [15,58]. Researchers identified additional factors such as tire width, tire pressure, and the rubber's modulus, as significant contributors to the tire-pavement contact behaviour [17,56,59].

Recent studies have found the effect of directional characteristics of the pavement texture, traffic direction, and polishing effect on tire penetration depth [60,61]. As a result of the repetitive traffic polishing occurring consistently in one direction on the pavement, disparities in surface irregularities may emerge within both acceleration and

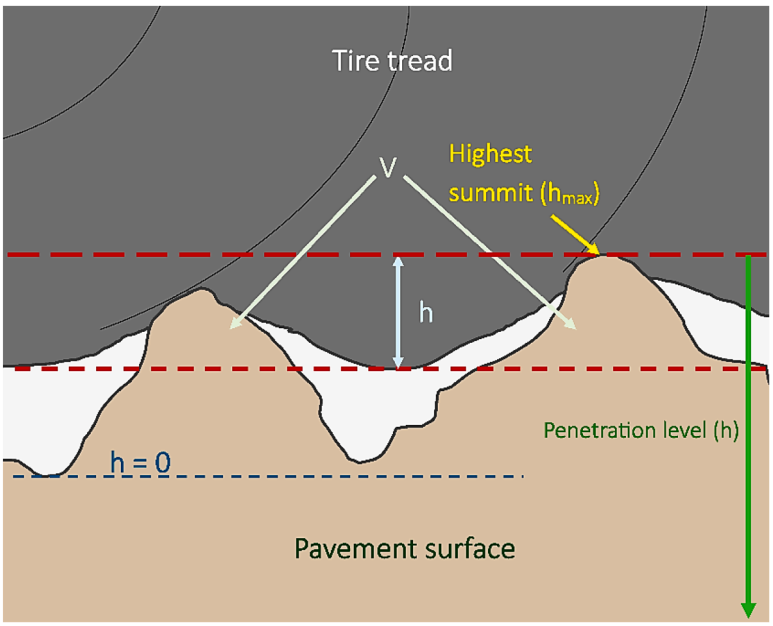

Fig. 1.1. Schematic illustration of tire penetration depth (h) and penetration volume (V) within the tire-pavement contact zone. The highest surface summit (h_{max}) defines the reference level, and the penetration depth (h) is measured between the tire tread and pavement surface relative to this level.

deceleration zones along all the wheel paths of the pavement. Consequently, it becomes evident that the point at which the normal tire load is applied also varies on the surface irregularities, thereby leading to differences in tire penetration.

As mentioned above various factors influence tire penetration levels, however, estimating penetration depths remains a challenge. Rresearchers speculated penetration depths by using the texture parameters and 2D enveloped texture profile [62–64]. The corresponding enveloped texture profiles were generated through an enveloping algorithm [63, 64]. The enveloping techniques neglected the impact of loads, material properties, and only the peaks of the curve they produced overlay with the pavement texture profile. Ejasmont et al. [15] was conducted a study between rolling resistance and MPD by using an enveloping method together with classical MPD approach. It was found that both approaches provide weak agreement in relation to coefficient of rolling resistance. It could be because the 2D enveloping technique completely ignores the effect of real-world conditions on the entire tire contact patch with the surface. Therefore, in order to addresses the described drawbacks, the following research goal and scope are developed in this study.

1.2. Research goal and scope

The aim of the study is to develop a methodology that combines both data-driven and physics-driven approaches to improve the prediction of rolling resistance by considering the relationships among rolling resistance, the δ parameter, and texture properties. The proposed framework is developed using popular ML models, including multiple linear regression (MLR), random forest regressor (RFR) and Artificial Neural Networks (ANN), as the models are widely used in the literature [65–70]. The framework incorporates commonly available smartphone-based computer vision technology to capture δ parameter and texture properties from field video recordings. To the best of the authors' knowledge, obtaining accurate tire-pavement interaction parameter is still a challenge for both tire-pavement industries. In order to address above challenges, aim and scope of the research is defined as follows:

- To develop a system using video-based computer vision technology for reproducing digital replicas of pavement surfaces. The primary focus is to create a cost-effective, user-friendly, and reliable system by using smartphone videos which is capable of measuring key surface properties and physics-based parameters, namely δ parameter.
- To investigate the relationship between rolling resistance and surface texture properties derived from historical data and the approach described in (i). The data is collected from the Dutch pavement network. This step focuses on laying the foundation for developing data-driven models and assessing prediction accuracy without incorporating δ parameter.
- To design a simple portable device capable of capturing δ parameter on the consistence pavement sections as mentioned in (ii). The verification of the data is conducted using an MTD digital calculator and a computer vision technique.
- To develop static numerical models simulating tire-pavement interaction for measuring δ parameter. The development and validation of the numerical models are conducted using field-measured data described in (i) and (ii). The main focus on this step is to deepen the understanding of δ parameter's behaviour under varying loading conditions.

1.3. The innovative aspect of the research

The innovative aspects of the research are highlighted below:

- *Video-based digital replica system:* the research introduces a novel, cost-effective system using smartphone-based computer vision technology to create digital replicas of pavement surfaces. This approach combines affordability, ease of use, and reliability, making advanced pavement surface analysis more accessible compared to existing high-cost, specialized equipment.
- *Integration of physics-based parameters to data-driven models:* by leveraging data from the Dutch pavement network, the research establishes a robust approach for developing data-driven models combining the δ parameter to predict rolling resistance. The incorporation of δ parameter, which have not been measurable with any existing equipment. Additionally, the parameters have not been examined in any previous studies. This research develops a portable

device specifically designed to measure δ parameter, which represents a significant advancement in pavement analysis. It offers a new way to enhance the accuracy of rolling resistance predictions and it is also applicable to other studies investigating tire-pavement interactions.

- *Numerical modelling for measuring the δ parameter:* the development and validation of 3D numerical models to simulate behavior of δ parameter under static and varying loading conditions. This aspect not only supports to reproduce the field measurements of the δ parameter, but also offers insights into their application in diverse real-world scenarios related to tire-pavement interaction.
- *Enhanced prediction accuracy and comprehensive multi-method approach:* the research investigates the added value of δ parameters in improving rolling resistance prediction accuracy by integrating the parameters into data-driven models. Additionally, it adopts a comprehensive multi-method approach, combining video-based digital replica system, field measurements with portable device, and numerical modelling. This integrated framework hopes to provide a better understanding of pavement properties and their influence on rolling resistance, paving the way for future advancements in pavement engineering.

2. Research methodology

As illustrated in Fig. 1.2, the study was conducted in seven main phases. Phase I was involved field measurement of the δ parameter. In Phase II, a reproduction of the 3D pavement surface was conducted. Phase III was focused on obtaining relevant surface texture properties using Laser Crack Measurement System (LCMS) data and the system developed in Phase II. During Phase IV, a Finite Element (FE)-based tire-pavement interaction model was developed and validated against scaled experiments conducted with the developed device using a 10×4.5–$5''$ tire and texture pads. In Phase V, the validated model was upscaled to simulate full size tire (Standard Reference Test Tire (SRTT P225/60R16) [71]) loading conditions and calculated corresponding δ parameter. The δ parameter was calculated under testing conditions similar to the conditions used for measuring rolling resistance data with TU-Gdansk's RR measurement trailer [23,72]. Phase VI was evaluated the rolling resistance prediction accuracy by developing data-driven models incorporating the δ parameter calculated in Phase V. Finally, in Phase VII the results and conclusions based on the outcomes from Phase VI was compared. A detailed description of the tasks performed in each phase is provided below:

2.1. Phase I: definition of δ parameter and its measurements

As shown in Fig. 1.2, in Phase I, a portable device was built to measure the δ parameter for a given pavement surface. A test tire with similar characteristics to the tire used for measuring rolling resistance (RR) in Phase VI was utilized to build the device. A polymer-based texture pad was used to measure the δ parameter. More details about the device are described in following sub-sections. The texture pads were used to calculate the δ parameter by incorporating the Python-based toolkit developed in Phase II. The measurements of δ parameter was used to validate the FE numerical models in Phase IV. The validation measurements in Phase IV were collected at a Dutch pavement test section called INOVA.

2.1.1. Calculation of δ parameter

As shown in Fig. 2.1, the δ parameter, which is a function of tire-related properties, pavement-related properties, contact properties, and operational conditions, can be expressed as given in Eq. (1.1):

$$\delta = f\left(P_{tire},\ P_{pavement},\ P_{contact}, P_{operation}\right). \tag{1.1}$$

The $\delta_1,\ \delta_2, \ldots, \delta_i$ express individual δ parameter with respect to reference level ($\delta_0 = 0$) of "highest summit" (see Fig. 2.1) on the surface morphology. The δ parameter is characterized by the average depth of tire-rubber penetration within the contact patch in relation to the surface morphology, as defined in Eqs. (1.2) and (1.3):

$$\delta = \ \delta_{avg} = \ \frac{1}{n} \ \sum_{i=1}^{n} \delta_i, \tag{1.2}$$

where

$$\delta_i = |h_0(x,\ y) - \ h_{rubber}(x_i,\ y_i)|. \tag{1.3}$$

Here, n denotes the number of discrete points within the tire contact patch where the penetration depth is measured; δ_i denotes the individual tire penetration depth in relation to surface texture at a specific point $(x_i,\ y_i)$ on contact patch; δ_{avg} denotes the average of tire penetration depths; $h_{rubber}(x_i,\ y_i)$ denotes the deformation depth of the tire rubber at the point $(x_i,\ y_i)$; $h_0(x,\ y)$ denotes the surface texture-induced reference depth at a point $(x,\ y)$ corresponding to the highest summit; P_{tire}, $P_{pavement}$, $P_{contact}$, and $P_{operation}$ denote tire-related properties, pavement-related properties, contact characteristics, and operational conditions, respectively.

As presented in Fig. 2.1, the rolling resistance arises from the cumulative effect of all micro and macro-contacts, including regions of extreme penetration. Since the mean penetration depth accounts for these extremes, it offers a more physically representative measure of the tire's energy loss due to deformation, which directly correlates with rolling resistance. Therefore, the mean δ parameter across the contact patch was assumed to adequately capture the overall tire-pavement interaction.

In this study, $h_0(x,\ y)$ is defined as the global maximum elevation within the analyzed tire contact patch, extracted from the reconstructed three-dimensional surface after preprocessing. Hence, it does not represent a locally fluctuating peak at each coordinate, neither it is defined by the edges of individual surface voids. The 3D surface obtained from SfM or LCMS data was subjected to mesh refinement and radius-based outlier removal to eliminate scanning noise and isolated artifacts. The reference level ($\delta_0 = 0$) was then determined as the highest surface elevation within the filtered contact patch domain. For porous asphalt surfaces containing voids, this definition ensures that deep cavities or void bottoms do not influence the reference plane, since they lie below the highest summit level. Furthermore, because the δ parameter is calculated as the average penetration depth over n discrete points within the contact patch (Eq. (1.2)), local geometric fluctuations caused by surface voids have limited influence on the overall δ value. This approach provides a stable and physically consistent reference for evaluating tire penetration depth across different surface morphologies.

Rolling resistance is fundamentally governed by viscoelastic hysteresis occurring under dynamic rolling conditions [13,73], where energy dissipation depends on both frequency-dependent material loss properties and deformation amplitude. The δ parameter introduced in this study does not aim to directly quantify dynamic hysteretic energy. Instead, δ represents a physics-informed geometric contact-conformity metric describing the mean penetration depth of the tire tread into the pavement texture under a given normal load. In viscoelastic rolling systems, dissipated energy per cycle depends on both the material loss behaviour and the magnitude and spatial distribution of strain excitation imposed by surface texture. Within this framework, δ serves as an indicator of texture-induced deformation severity that contributes to hysteretic losses by governing the deformation-amplitude component of the interaction. The present static formulation captures this geometric deformation component, while frequency and temperature-dependent viscoelastic effects remain outside the scope of this study.

2.1.2. Development of the δ parameter measuring device

A portable device was built (see Fig. 2.2) to measure the δ parameter for a given pavement surface section in INOVA test section. The test

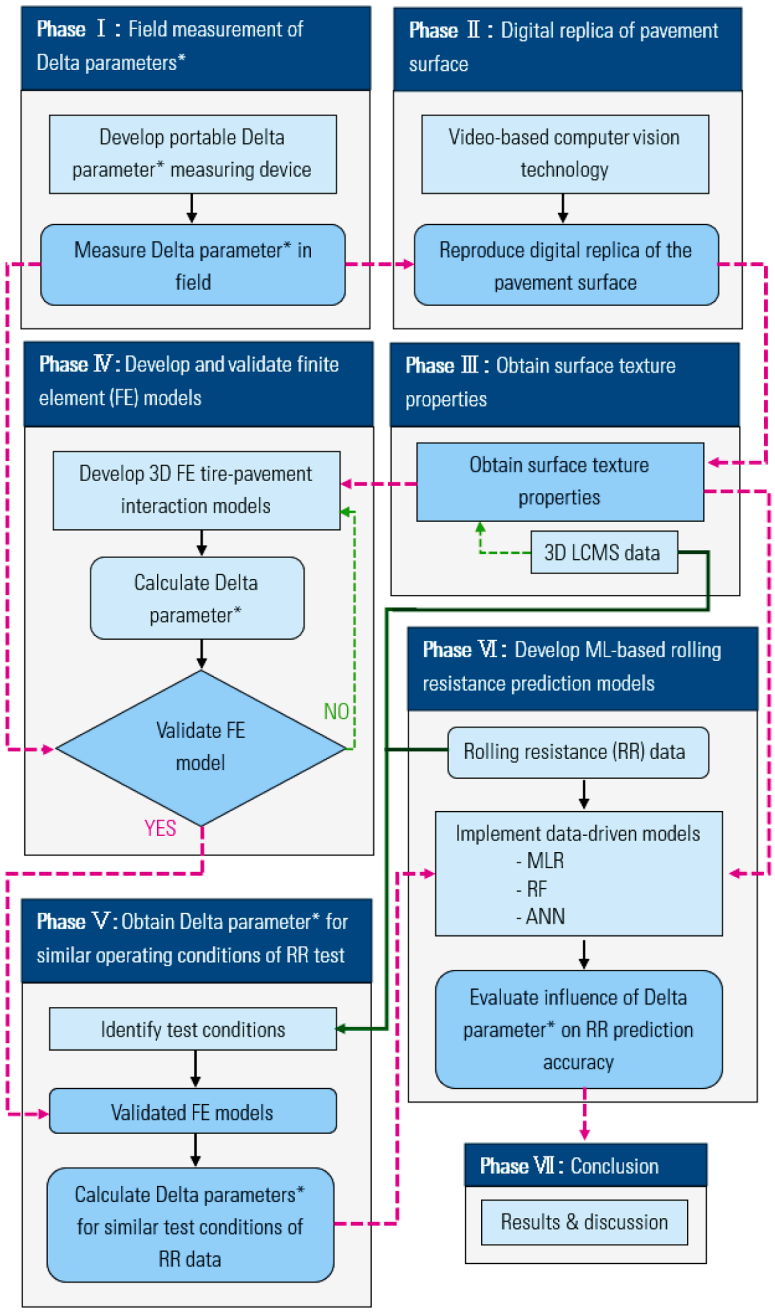

Fig. 1.2. Research framework[1].

[1] *See sub-Section 2.1

section was built with DLPAC 16 layer [74,75] (see Table 2.1 for expanded form of the acronym). The machine was designed to bear loads of up to 50 kg. This approximate load was found to represent most of the passenger car tire range. In this research easily available tire, sized $10 \times 4.5–5''$ with pressure of 100 kPa was used. It is noted that other type of similar size of tires can also be replace in the system. The components of the device were designed and fabricated at TU Delft using the 3D printing facility. FE simulations were carried out in order to analyse the stress distributions and assess the stability of the device. The design includes a rigid loading frame, a tire mounting platform, and a vertically sliding loading plate capable of applying a static force to the tire axle.

The δ parameter was derived from measurements taken under static loading conditions, based on the assumption that the static load approximates the average tire-pavement interaction during typical vehicle operation. Although tire-pavement contact is inherently dynamic, conducting static tests simplifies the complex loading scenario, reduces the need for sophisticated instrumentation, and avoids controlled environments that are often impractical for in-field measurements. Thus, static testing was employed as a practical compromise to obtain reliable and repeatable penetration data within the constraints of field conditions.

The loading mechanism ensures uniform pressure distribution, simulating the real-world static loads experienced by tires on pavement. In order to measure the δ parameter, a thin layer of polymer material was used. As illustrated in Fig. 2.2, a polymer-based material (texture

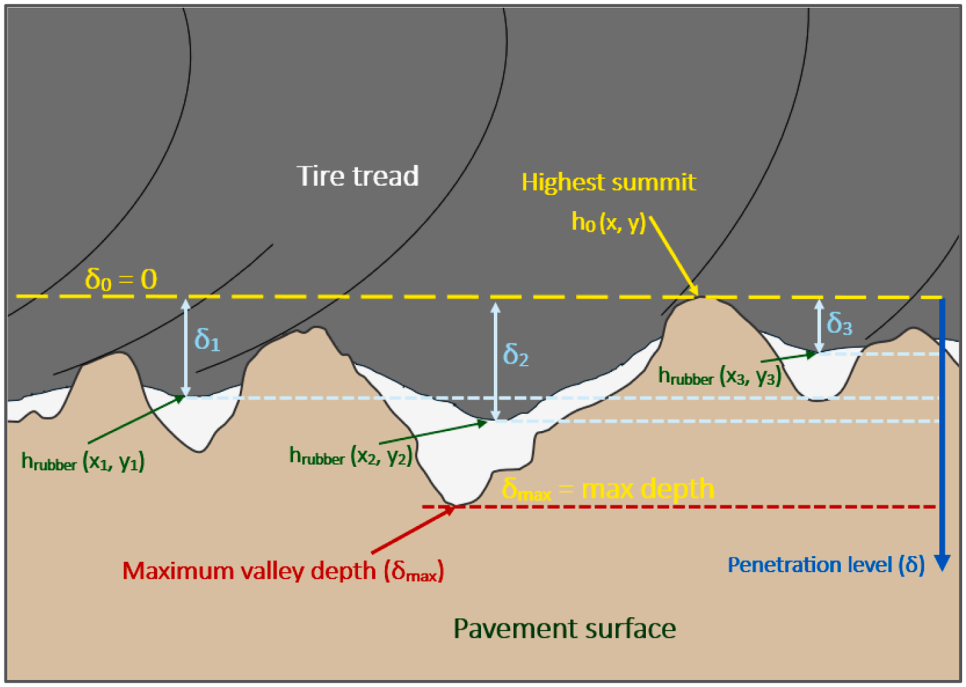

Fig. 2.1. Schematic visualization of the δ parameter representing tire-rubber penetration into pavement surface texture. The highest surface summit is taken as the reference level ($\delta_0 = 0$), and individual penetration depths (δ_1, δ_2, δ_3) are measured between the tire tread and the surface morphology within the contact patch. The maximum valley depth (δ_{max}) and the average penetration level (δ) are illustrated.

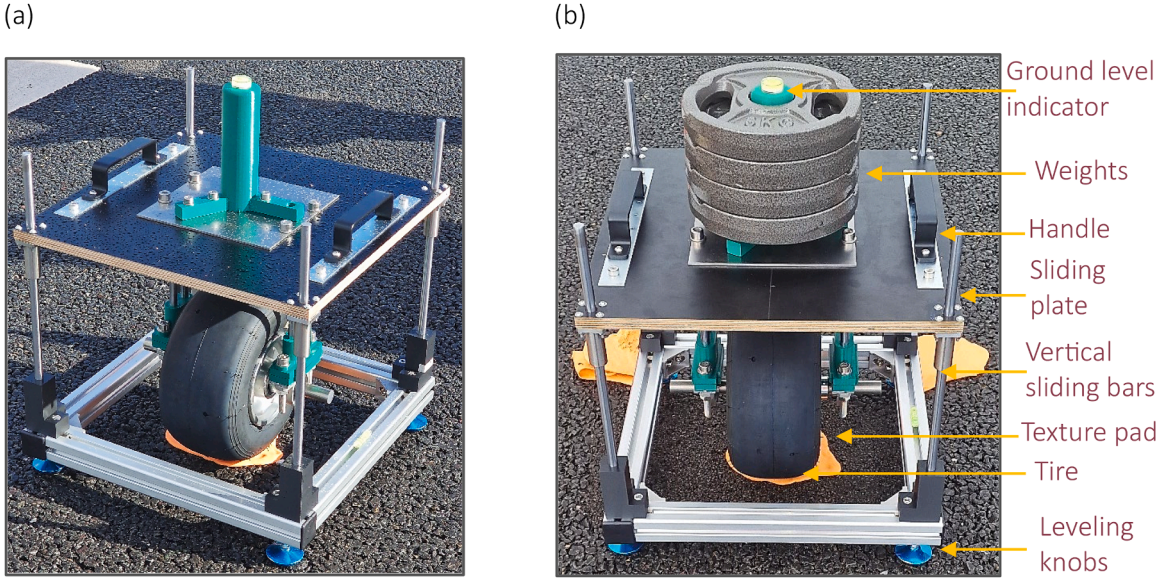

Fig. 2.2. Developed device for measuring the δ parameter and tire penetration pattern under loading level of 343 N: (a) Device without load, (b) Device with load and its elements.

Table 2.1
Description of PA16 pavement sections [74,75].

Acronym	Expanded form (English)
DLPAC	Dual Layer Porous Asphalt Concrete
ZOAB	Porous Asphalt
ZOAB+	Porous Asphalt +

pad) was placed between the tire and the pavement surface to measure tire penetration. A Python-based toolkit was developed and digital replicas of the texture pads were used to calculate the δ parameter. The composite polymer material of the texture pads was prepared to have a similar range of superficial hardness as the tire tread rubber. Although the polymer texture pad was selected to have properties comparable to tire tread rubber, it is highlighted that tire rubber exhibits complex hyper-elastic and viscoelastic behaviour that cannot be fully replicated by the pad material. The primary purpose of the texture pad in this study is not to replicate the full constitutive response of tire rubber, but to capture the geometric imprint of tire penetration under controlled static loading conditions. In other words, the pad functions as a geometric transfer medium to record the tire deformation imprint as an average parameter within the contact patch. It is important to note that an exact

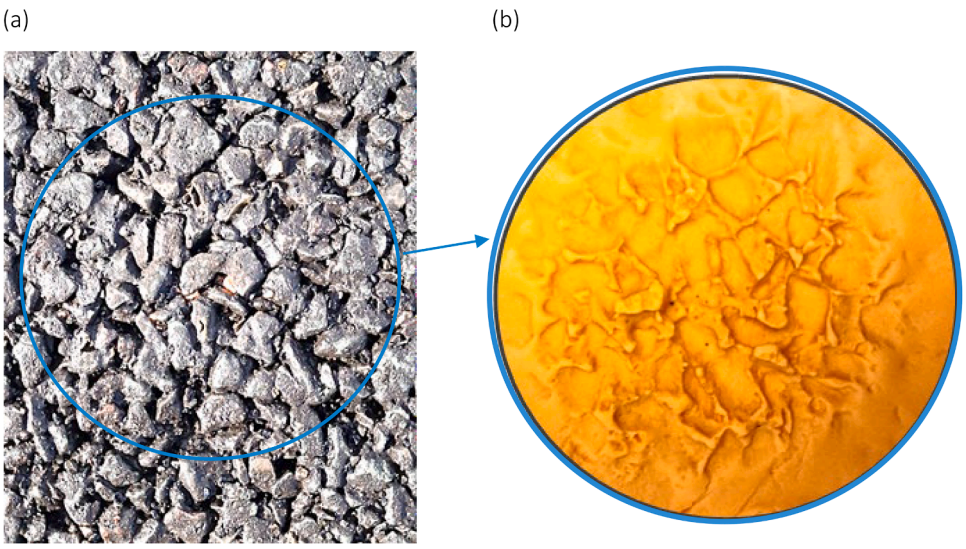

Fig. 2.3. Tire penetration pattern under loading level of 343 N: (a) Pavement surface at INOVA test section, (b) Corresponding texture pad with negative texture (Expanded view).

match between the mechanical characteristics of the texture pad and the wide range of tire tread materials used in practice is difficult to achieve. Tires vary significantly in compound composition, tread hardness, and structural properties, while the preparation of polymer pads can also be influenced by curing time and environmental conditions in field. For this reason, the texture pad material was designed to approximate the hardness range of tire tread rubber rather than to reproduce its full mechanical behaviour. Texture pad layers with a thickness of 1.5–2 mm was used to capture the δ parameters of the application. Fig. 2.3 shows the typical (negative texture) depth pattern that was obtained under a 30.5 kg load and an equivalent pressure of 100 kPa. The measured δ parameter values were utilized to validate the δ parameter captured from FE numerical models, as presented in Phase IV.

In this study, the δ parameter is obtained using a static loading approach because direct measurement of a dynamic δ parameter under rolling conditions is not feasible with the current field measurement setup. A possible future approach involves determining the dynamic δ parameter through fully coupled computational modelling of tire-pavement interaction. Such simulations require transient rolling contact analysis with frequency-dependent viscoelastic material characterization and substantial computational resources, which are beyond the scope of the present study.

2.2. Phase II: acquisition of digital replicas of pavement surfaces with texture properties

In Phase II, video-based computer vision technology was used to generate digital replicas of given pavement surfaces and texture pads samples from Phase I. The Structure from Motion (SfM) technique was applied to recorded videos of the surface samples to generate the replicas. The video footage of the target surface was recorded under uniform lighting conditions to minimize shadows and reflections that could affect feature detection. Videos were captured at a resolution of 3840 × 2160 pixels (4 K UHD), with an aspect ratio of 16:9 and a frame rate of 60 frames per second (fps), ensuring preservation of fine spatial details and minimizing motion blur. Each recording session lasted approximately 40–60 s, resulting in sufficient frame density for robust feature matching during SfM reconstruction. The camera was moved smoothly around the sample along a semi-circular or orbital path to capture multiple viewpoints. The distance between the camera and the surface was maintained approximately constant to preserve scale consistency across frames. The camera was positioned at angles between 30° and 60° relatives to the surface normal, which ensured optimal visibility of surface texture variations while minimizing perspective distortion. Both horizontal and slightly elevated viewpoints were included to provide adequate overlap between consecutive frames, supporting reliable geometric reconstruction.

Data preprocessing was carried out to perform mesh refinements, data cleaning and data scaling. Poisson surface reconstruction was employed to generate meshes with triangular elements and refine the surface topology from noisy point clouds. The radius outlier removal technique was applied to eliminate points with insufficient neighbouring data within a specified radius. Subsequently, the mesh coordinates were rescaled to standard units to ensure consistency across all datasets. The purpose of the data preprocessing stage was to ensure the quality of the gathered data while also enabling correct transformation for further analysis in Phase III and IV. The replicas were validated using sand patch test and Python-based MTD digital calculator. As presented in Fig. 2.4, a video-based computer vision technique was used to develop digital pavement surface models. The tool was developed using an in-house built Python framework, incorporating the commonly used SfM technique [76–78].

A horizontal resolution of approximately 0.5–1.0 mm after scaling and mesh refinement was achieved using the SfM reconstruction. This resolution is adequate for determining macro-texture indicators such as MPD, which are defined over millimetre-scale surface wavelengths. The reconstructed surface models were validated against sand patch test measurements and a digital MTD calculator, showing deviations within acceptable engineering tolerance. Therefore, the precision of the computer vision approach is sufficient for δ parameter determination at the macro-texture scale considered in this study. Further details regarding the development, calibration, and validation of the digital reconstruction approach and the MTD calculator are provided in a separate study by the authors, where the methodology is discussed comprehensively.

As illustrated in Fig. 2.4(a), the recorded video was then converted into a 3D textured digital model using the developed framework. Subsequently, the corresponding mesh of the surface (see Fig. 2.4(b)) was generated. Mesh refinements were performed to ensure the quality of the mesh using an open-source 3D creation suite [79]. The improved mesh was then used to develop relevant FE-based tire-pavement interaction models, as described in Phase IV. Additionally, the in-house built Python framework was employed to calculate surface texture indicator such as MPD. The acquired readings of the indicator were used in Phase VI and Phase III.

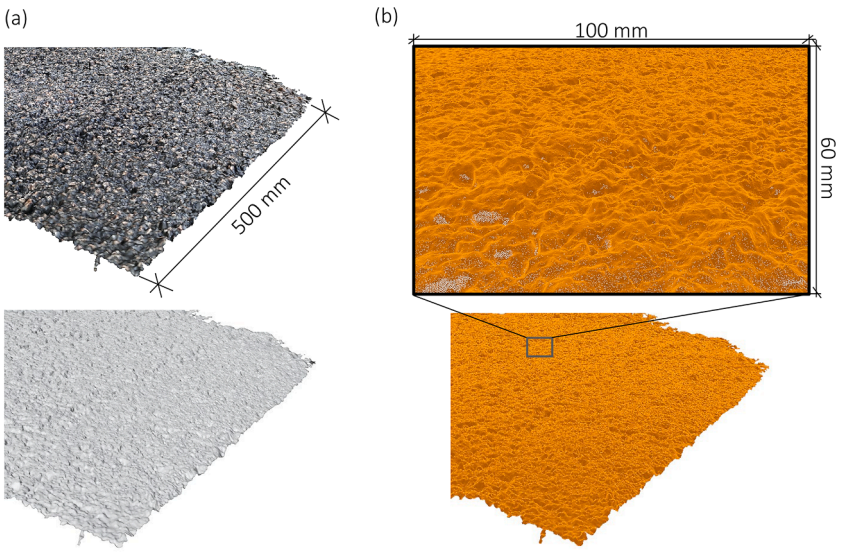

Fig. 2.4. Digital replica of porous asphalt surface sample: (a) Digital representation of the pavement surface and (b) Digital representation of the pavement surface with mesh.

2.3. Phase III: measurements of rolling resistance and texture properties

In Phase III, the relevant surface texture properties such as MPD, were obtained with the help of the Python-based toolkit developed in Phase II. To expand the surface texture dataset, 3D pavement surface data from the Laser Crack Measurement System (LCMS) were incorporated. It is noted that the 3D data were collected from the same pavement sections where rolling resistance data were measured. The extended dataset was used as input to develop data-driven models in Phase VI. Additionally, the LCMS data were used to calculate the δ parameter by extending the validated FE models from Phase IV.

Sections with PA16 (ZOAB / ZOAB+) were chosen to measure both RR and 3D LCMS data, because PA16 is the most common asphalt top layer used on highways in the Netherlands (see Table 2.1). The required 3D pavement surface data were collected using LCMS measurements [80], which were gathered from pavement surfaces of DLPAC 4/8, DLPAC 0/5, New PAC 16, and Worn PAC 16. The relevant texture indicators including MPD, root mean square (RMS), Skewness, estimated texture depth (ETD) were calculated using LCMS measurements. The measurements were performed using a mobile system traveling at a speed of 80 kmh^{-1}, which detailed 1 mm resolution. Surface texture data were recorded simultaneously with the rolling resistance measurements. Further details about LCMS can be found in [81].

To measure RR, TU-Gdansk's RR measurement trailer [23,72] was utilized at a speed of 80 kmh^{-1}, as recommended by prior studies [82]. The SRTT tire [71] was fitted to the trailer and inflated to a pressure of 210 kPa. The study covered 22 PA16 pavement sections, where both rolling resistance and texture data were gathered concurrently. It is noted that the selected pavement sections varied in age and maintenance conditions. Measurements were conducted over a 500 m length on each of the 22 sections with a total of 12 measurement runs, resulting in a total of 22,236 samples of data. Each test included a warm-up process for the tire to ensure temperature stabilization, material flexibility, and pressure equalization, thereby guaranteeing consistent and reliable results. Tire pressure and temperature were continuously tracked during the tests using a sensor attached to the tire, which transmitted data wirelessly to the data acquisition system. The tracking setup enabled real-time monitoring and adjustments to tire pressure with the sensor providing precision within ±1 kPa. Since tire pressure was actively monitored, no manual adjustments were required during the measurements. During the measuring process average temperatures of tire, road and surrounding air was measured as 25.5 °C, 22.3 °C and, 14.9 °C, respectively. Further details of the RR measurement approach can be found in [83]. The measured data in Phase III were used in Phase IV to develop the corresponding FE models.

2.4. Phase IV: development of static finite element models of tire-pavement interaction

In Phase IV, static FE models of tire-pavement interaction were developed and validated to measure the δ parameter under different loading conditions. The FE model was implemented under conditions similar to the test setup mentioned in Phase I. In this phase, the test tire and surface conditions related to Phase I were numerically modelled. The developed FE model was validated by comparing the δ parameter obtained infield during Phase I under similar testing conditions. The validated FE model was subsequently modified in Phase V to calculate the δ parameter under similar testing conditions to the measured rolling resistance data.

The development of the FE model for static tires on pavements involves a systematic approach to accurately simulate tire behaviour. The FE model in this Phase, consisting of a tire and a textured single-layered pavement surface which was generated from Phase II. A commonly used FEM package was utilized to develop the static tire-pavement interaction FEM model [84]. The authors used key components of the pneumatic tire as shown in Fig. 2.5 with hyper-elastic material properties to build the FE model.

As illustrated in Fig. 2.6, the rubber components of the tire were modelled using C3D8H 8-node linear brick elements [84], while the bead sections were created with C3D8 8-node linear brick elements. The carcass parts were constructed using M3D4 4-node quadrilateral membrane elements, and the pavement section was developed using C3D4 4-node linear tetrahedron elements. Uniaxial compression and shear tests were conducted to obtain relevant mechanical properties of the tire rubber. On the basis of the test data, Neo-Hookean hyper-elastic material model was found as the best fitted material model of the particular tire rubber. Fig. 2.7 presents the comparison between the measured and predicted responses in terms of force-displacement (uniaxial compression) and stress-strain (shear) relationships. Furthermore, the Neo-Hookean predictions showed good agreement with the experimental data, indicating that the selected model adequately captured the nonlinear mechanical response of the tire rubber and was suitable for the developed finite element simulations. The constitutive equation of used material model is expressed in Eq. (2.1) [84]. The remaining

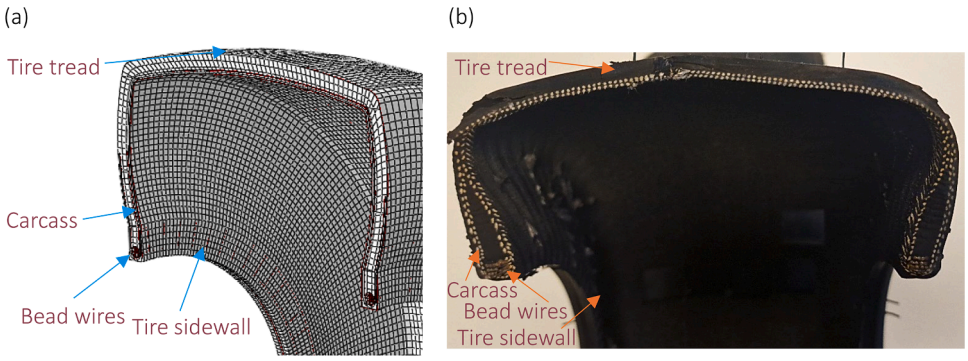

Fig. 2.5. Cross sectional view of the tire including its components: (a) 3D FEM model of the tire and, (b) Actual profile of the tire sized 10 × 4.5–5″.

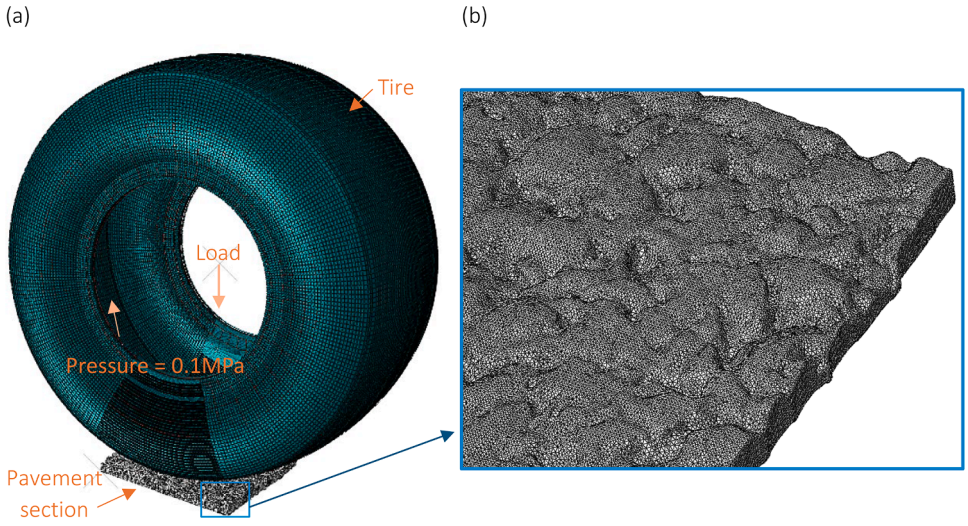

Fig. 2.6. FE model of tire-pavement interaction: (a) 3D Static FEM model and, (b) 3D reconstructed pavement section.

material properties of the tire components were gathered from the past studies [85,86]. The typical steps outlined in previous studies were followed to build the 3D static FEM model by assigning necessary interactions and relevant constraints [84,86–88].

The constitutive equation of Neo-Hookean hyper-elastic material model is presented in Eq. (2.1):

$$U = C_{10}(\bar{I}_1 - 3) + \frac{1}{D_1}(J_{el} - 1)^2. \tag{2.1}$$

where, U represents the strain energy, $\bar{I}_1$corresponds to the first invariant, C_{10} and D_1 are material properties that depend on temperature, J_{el} refers to the elastic volume ratio. Based on the test data, the C_{10} coefficient was calculated as 7.9842. In the FE tire-pavement interaction models, surface-to-surface contact [73,89–91] was defined between the tire tread and pavement surface. The normal contact behaviour was modelled using a hard contact formulation, preventing interpenetration under compression while allowing separation. The tangential behaviour was implemented using a penalty-based friction formulation with a friction coefficient (0.7) representative of dry asphalt-rubber interaction.

In order to ensure the accuracy and numerical stability of the developed FE model, a mesh convergence study was conducted for the tire-pavement interaction model. It was essential to verify that the solution was independent of mesh density because the calculated δ parameter is directly derived from the predicted vertical deformation response. Fig. 2.8 presents the variation of maximum vertical deformation with respect to the total number of elements in the model. As shown, the predicted deformation decreases with mesh refinement and gradually approaches an asymptotic value. Beyond approximately 1720,000 elements, the change in maximum vertical deformation became negligible (variation less than 1% between successive refinements), indicating that mesh convergence had been achieved. Based on this convergence assessment, a mesh consisting of 1725,751 elements was selected for the final simulations. The main purpose of this Phase was to ensure the accuracy of the proposed methodology for calculating the δ parameter both numerically and in the field. In Phase V, the validated FE model in Phase IV was subsequently modified to calculate the δ parameters under testing conditions similar to those used for the measuring the rolling resistance data in Phase II.

2.5. *Phase V: improvement of finite element models to obtain δ parameter for similar operating conditions of rolling resistance test*

In Phase V, δ parameter was measured under similar test conditions as the measured rolling resistance data by utilizing the validated models from Phase IV. The surface condition of the validated FE model was modified by using 3D LCMS data in Phase III. This step was carried out to measure the δ parameters under comparable surface and test conditions, such as the applied load of the measured rolling resistance. The measurements were used as physics-based input parameter in Phase VI.

In this Phase, the validated FE model in level one was modified by changing relevant tire parameters, pavement surface characteristics and tire operating conditions. The modifications included incorporating a comparable test surface based on 3D LCMS data, switching the tire to a SRTT tire, adjusting the inflation pressure to 210 kPa, and setting the loading condition to 4000 N (see Fig. 2.9). The steps were repeated in

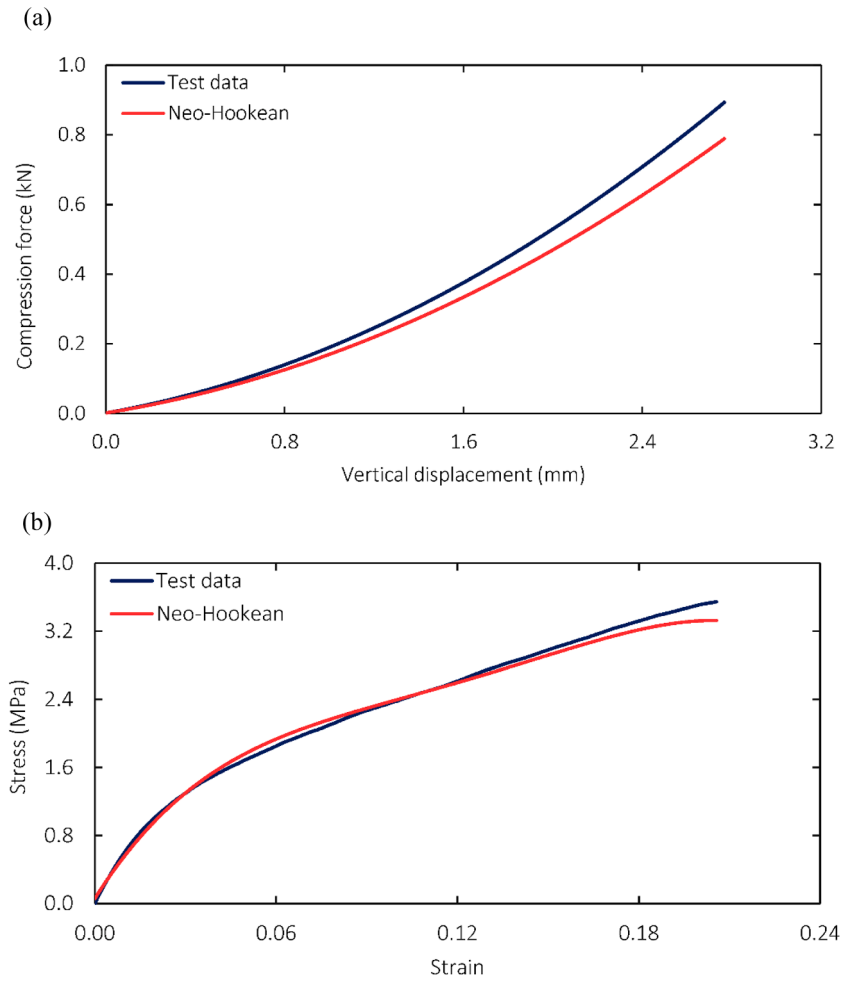

Fig. 2.7. Comparison between experimental data and Neo-Hookean hyper-elastic material model predictions for (a) uniaxial compression (force-displacement response), and (b) shear test (stress-strain response).

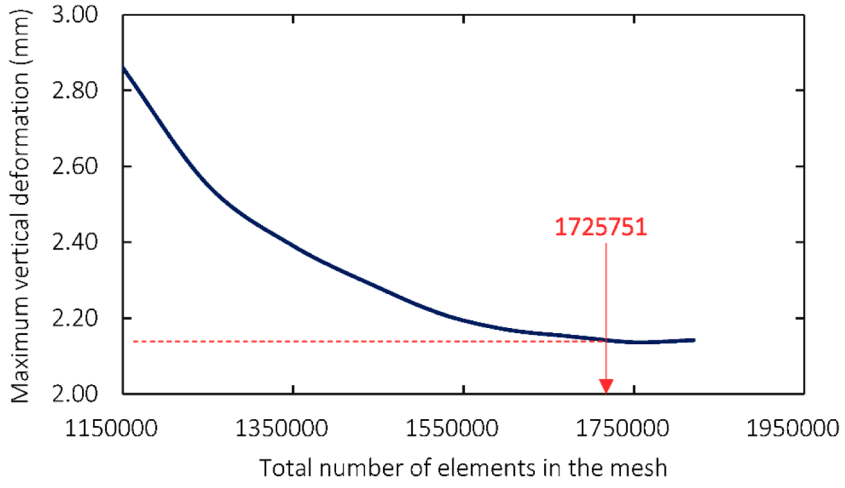

Fig. 2.8. Mesh convergence study.

the level one to develop the modified FEM model. The relevant material properties for the tire components were obtained from a past study [92]. The modified static FE tire-pavement interaction model consists of a total of 2724,785 elements.

It is noted that the portable device developed in Phase I utilizes a small-sized tire, whereas rolling resistance measurements were conducted using a full-scale SRTT tire. The transition from the small tire configuration to the SRTT configuration was achieved through validated FE upscaling, where tire geometry, inflation pressure, loading conditions, and material properties were modified to replicate the RR testing setup. Direct experimental measurement of the δ parameter using a full-scale SRTT tire in field conditions would require a large-scale loading

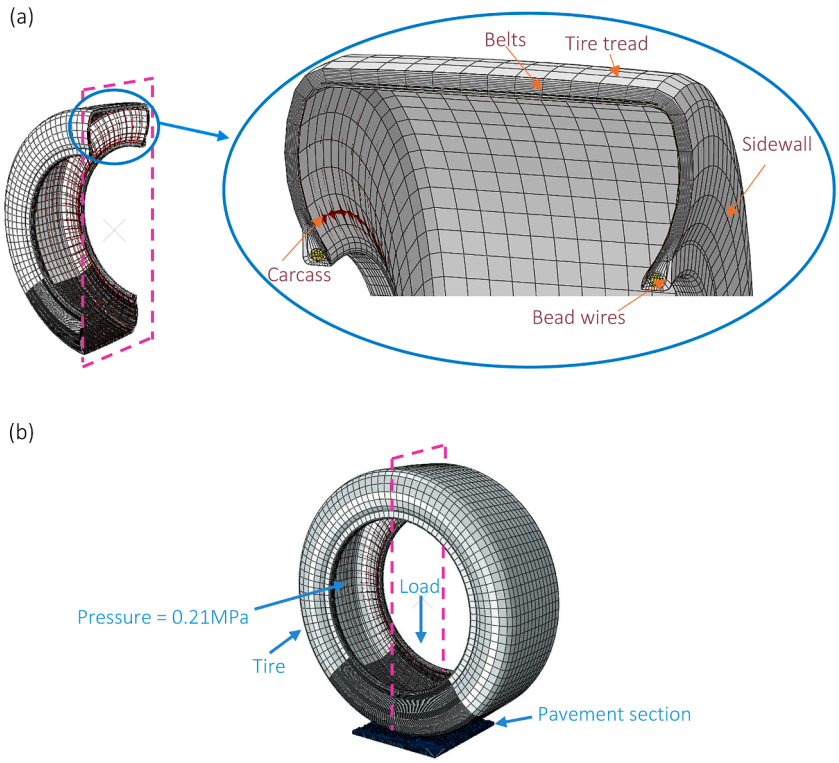

Fig. 2.9. FE tire-pavement interaction model with tire SRTT: (a) Cross-sectional view showing structural components (tread, belts, carcass, sidewall, and bead wires) of SRTT tire and mesh discretization and, (b) 3D static FE setup illustrating tire inflation pressure (0.21 MPa), applied vertical load, and contact with the pavement section.

apparatus and controlled instrumentation, which were beyond the logistical and practical scope of this study. The purpose of the small-scale device was to establish and validate the δ parameter measurement methodology, which can be easily applied in both field and laboratory conditions. The corresponding full-scale behaviour was reproduced numerically under controlled boundary conditions.

The portable δ- measurement device and the LCMS-based approach operate at different scales within a unified methodological framework. The portable device was developed to experimentally establish and validate the δ parameter under controlled conditions and to calibrate the FE tire-pavement interaction model. After validation, the FE model was integrated with LCMS surface data to estimate δ under full-scale rolling resistance conditions. In practice, the portable device enables low-cost, project-level field measurement of δ where LCMS data may not be available, while the LCMS-FEM framework supports large-scale or network-level estimation. Together, they provide a multi-scale methodology linking direct physical measurement with broader predictive modelling.

2.6. Phase VI and phase VII: development of ML-based rolling resistance prediction models and assessment of results

In Phase VI, ML-based data-driven RR prediction models were developed by incorporating parameters from Phases III and V. Comparative analysis was conducted using three data-driven models: MLR, RF and ANN to evaluate the influence of the δ parameter on prediction accuracy of RR. In Phase VII, an analysis was conducted based on the results obtained from Phase I to Phase VI. Finally, based on the outcomes of Phase VI, critical assessments were conducted to evaluate the improved prediction accuracy of rolling resistance in relation to the δ parameter.

3. Verification and validation

Verification and validation are critical steps in the development of devices and models, ensuring both the accuracy of design and the reliability of performance under real-world conditions. The subsequent subsections present the specific approaches employed for verification and validation of the developed device and FEM models.

3.1. Verification of the device

The verification of the load-transferring capability of the device from the slider plate to the texture pad is crucial, as slight variations in force on the texture pad can result in over- or under-penetration. To assess the load-transferring performance from the slider plate to the texture pad, a simple weight scale-based approach was utilized. A digital weight scale with an accuracy of $\pm$0.05 kg was positioned between the tire and the ground. The initial load consisted of the self-weight of the slider plate, including the tire, which was 10.5 kg. Subsequently, an additional 5 kg was incrementally applied at each load level until a total of 35.5 kg was reached. The corresponding measurements from the weight scale were recorded at each loading level and plotted against the applied load, as presented in Fig. 3.1. The results indicate that the weight scale measurements closely align with the applied loads, demonstrating the reliability of the load-transferring mechanism of the device.

The verification and validation of the repeatability of negative texture on the texture pad were investigated using the verified device. As shown in Fig. 3.2(a) and Fig. 3.2(b), a self-weight test was conducted using a texture pad and a DLPAC core sample to assess the bearing capacity of the texture pad under its self-weight conditions. The results indicated that no negative texture formed on the texture pad under self-weight conditions, suggesting that the texture pad is activated only upon the application of an external load. Considering the verification of texture pad initial state, the repeatability of the negative texture on texture pad was investigated under three different loading conditions of

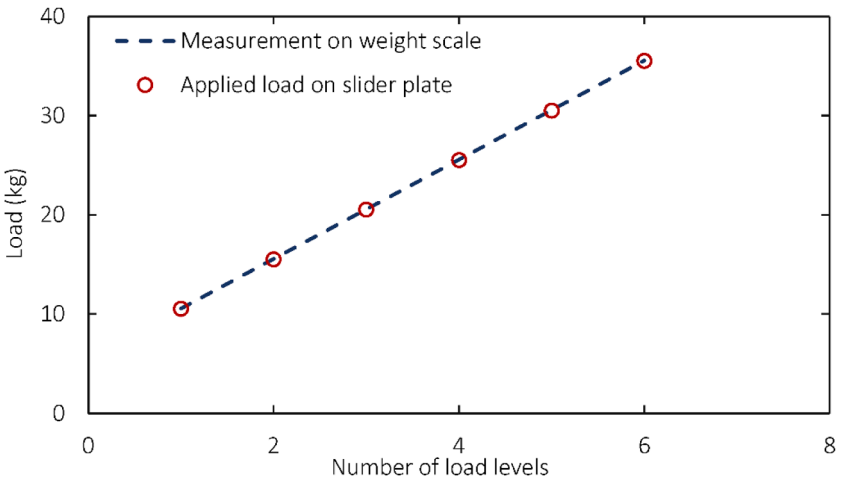

Fig. 3.1. Verification of device performance.

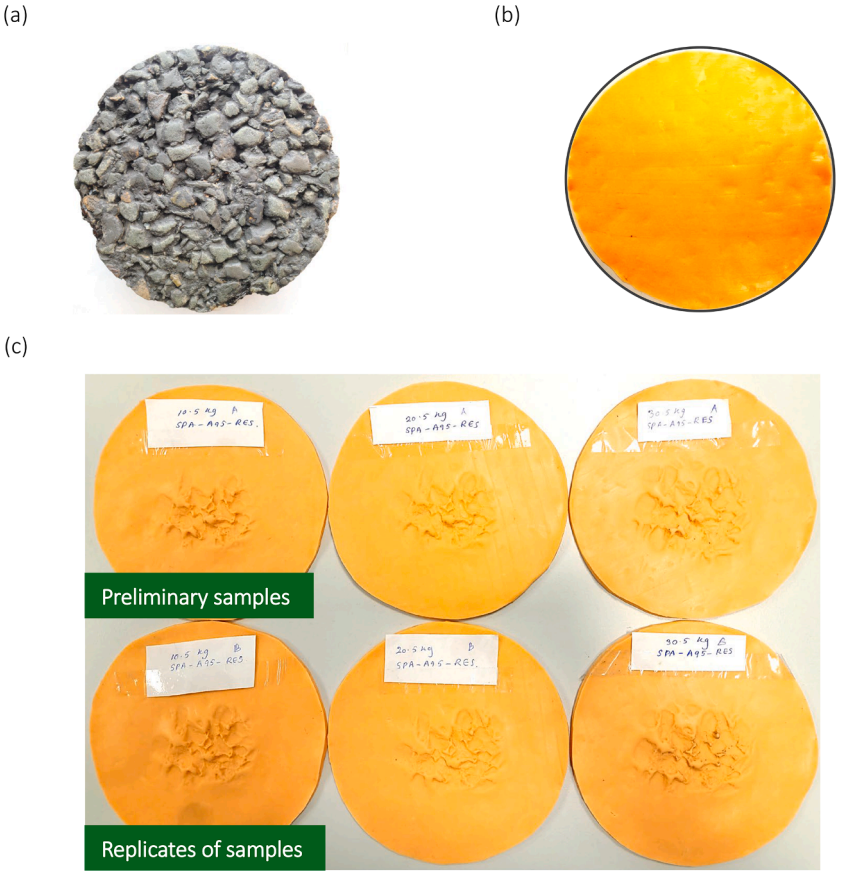

Fig. 3.2. Verification of negative texture repeatability: (a) Core sample with mixture type DLPAC16, (b) Texture pad under self-weight and, (c) Texture pads and their replicas under different loading conditions.

10.5 kg, 20.5 kg and 30.5 kg. As shown in Fig. 3.2(c), the area of the negative texture on both the preliminary and replicated texture pads increased in a similar pattern with the application of additional load. Furthermore, visual inspection revealed that the negative texture patterns of both texture pad samples were closely aligned, confirming the repeatability of the approach.

3.2. Validation of the FEM models

The validation of tire-pavement interaction FEM model was done by comparing experimental and predicted data of δ parameter. Experimental data were obtained from the developed portable device and in-field tests. The predicted δ parameter was generated by numerical models. The data were collected in both situations under static tire loads of 103 N and 343 N and using two types of pavement surfaces. Two different types of mixtures were considered in the INOVA test section to obtain the texture pads and measure the δ parameter (see Fig. 3.3). In addition to Mixture types 1 and 2, two additional mixtures, Mixture type 3 (DLPAC16 worn core sample) and Mixture type 4 (DLPAC_4/8 worn core sample) were used to broaden the validation scope and improve the

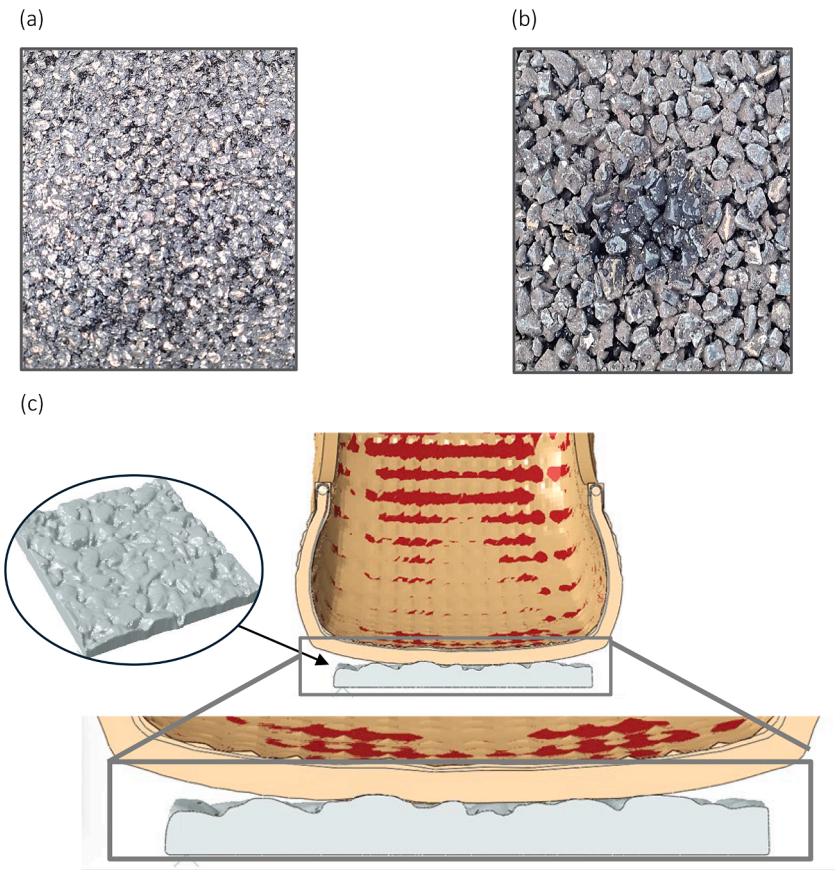

Fig. 3.3. Types of pavement surfaces and tire's contact patch: (a) Surface with mixture type 1, (b) Surface with mixture type 2, and (c) partially envelopment of the tire rubber over the peaks of the aggregates.

Table 3.1
Comparison of δ parameters and validation.

Type of the surface	Applied load (N)	δ parameter from in-field experiments (mm)	δ parameter from FEM simulations (mm)	MAE (mm)	MAPE (%)
Mixture type 1	343	3.44	2.95	0.17	7.19
Mixture type 1	103	2.17	1.86		
Mixture type 2	343	2.18	1.98		
Mixture type 2	103	1.61	1.39		
Mixture type 3	103	2.10	1.85		
Mixture type 3	152	2.21	2.08		
Mixture type 3	201	2.30	2.21		
Mixture type 3	250	3.30	3.21		
Mixture type 3	300	3.71	3.60		
Mixture type 4	103	1.62	1.51		
Mixture type 4	152	1.81	1.72		
Mixture type 4	201	2.00	1.95		
Mixture type 4	250	2.50	2.38		
Mixture type 4	300	2.80	2.72		

robustness of the analysis.

As shown in Fig. 3.3(a) and 3.3(b), the surface of mixture type 1 consisted of sharp peaks of aggregates, whereas the surface of mixture type 2 had more spread-out flat surfaces on the aggregates. As shown in Fig. 3.3(c), the tire rubber has partially enveloped over the peak of the aggregates.

Table 3.1 presents a comparison of the experimental results with the numerical modelling results. Mean absolute error (MAE) and Mean absolute percentage error (MAPE) was calculated by assuming all measurements represent the same physical quantity (δ parameter) under varying conditions. The MAE measures the average absolute difference between the experimental values and the FEM values. The MAPE measures the average percentage difference between the experimental values and the FEM values. As given in Table 3.1, the MAE value of 0.17 shows the FEM predictions are reasonably close to the experimental results. MAPE of 7.19% indicates that the FEM predictions are fairly accurate but could be improved. Considering the reasonable variations, the FEM models showed good accuracy.

The standard deviation of the residuals was calculated as 0.12 mm, which defined the uncertainty band of the FEM predictions ($\pm$0.12 mm). Assuming normally distributed residuals, the corresponding 95% confidence band was $\pm$0.24 mm. The majority of FEM predictions fell within this $\pm$0.24 mm interval, indicating stable and consistent model performance across different mixture types and loading levels. Although field-measured δ values were generally slightly higher than FEM predictions, the deviations remained within the calculated uncertainty bounds. The discrepancies were attributed to real-world factors not incorporated into the current numerical model, including ambient temperature variations and texture pad material interaction effects. The FEM model assumes idealized contact conditions and does not explicitly include pad stiffness or viscoelastic characteristics. Quantification of

these effects requires additional material testing and coupled contact modelling, which are beyond the scope of this study.

4. Results and discussion

This section presents and discusses the results obtained through the implementation of the described methodology. First, the relationships between the δ parameter, MPD and the type of pavement surface were analysed. Next, correlations between tire and pavement related parameters were analysed against rolling resistance using exploratory data analysis (EDA) techniques. Finally, the influence of the δ parameter on the prediction accuracy of rolling resistance was investigated for each data-driven model, including Multiple Linear Regression (MLR), Random Forest (RF), and Artificial Neural Networks (ANN).

4.1. Relationship between δ parameter and MPD

Table 4.1 presents the comparison of δ parameter and MPD readings with respect to four surface types. The results showed the lowest δ parameter of 0.11 mm and MPD of 0.89 mm for the DLPAC_0/5 pavement. The low δ parameter suggested a relatively uniform surface texture, while the low MPD indicated less pronounced surface features. Due to the DLPAC_0/5 pavement's composition of finer aggregates 0/5 mm, it typically exhibited a smoother surface texture with minimal depth and roughness. Based on the findings the surface was expected to have lower rolling resistance due to the smoothness.

The δ parameter and MPD of the DLPAC_4/8 pavement were higher than those of the DLPAC_0/5 pavement by 1.70 mm and 0.39 mm, respectively. The DLPAC_4/8 pavement, made up of medium-sized aggregates with a size range of 4/8 mm, showed a significant increase in both δ parameter and MPD. The larger aggregates resulted in a more pronounced surface texture with deeper grooves, increasing surface roughness. The higher δ parameter reflected greater variation in the texture profile and indicated a more pronounced effect on tire-pavement interactions compared to DLPAC_0/5. Based on the findings the surface was expected to have high rolling resistance compared to DLPAC_0/5 surface.

The New_PAC_16 pavement showed lower values for both the δ parameter (1.44 mm) and MPD (1.68 mm) compared to the Worn_PAC_16 pavement. The δ parameter of 1.44 mm, although smaller than that of DLPAC_4/8, still indicates a rougher surface than the finer mixes based on MPD values. The unpolished larger aggregates (16 mm) in the New_PAC_16 pavement create a more textured surface with deeper and more irregular profile depths. Based on the results the pavement indicated a greater influence on tire-pavement interactions and rolling resistance. The δ parameter (2.22 mm) and MPD (1.99 mm) of the Worn_PAC_16 pavement were higher than those of all the other pavement types. Wear and damage caused by traffic and environmental factors could be the reason for the significant increase in the surface roughness of the Worn_PAC_16 pavement. It is noted that the test section could be affected by distresses such as rutting, traveling, potholes, or cracking, which create additional cavities on the surface. The factors contributing to higher δ parameter and MPD values are further increase the surface texture and irregularity. The relationships indicates that larger and more worn aggregates such as those in Worn_PAC_16, contribute to significantly higher rolling resistance, which is an important consideration in pavement design and maintenance.

The δ parameter directly represents the spatially averaged penetration depth of the tire rubber into the pavement texture within the contact patch. In this study, δ values ranged from approximately 0.11 mm for smoother asphalt surfaces to approximately 2.22 mm for worn porous asphalt surfaces. These magnitudes are comparable to the measured MPD values (0.89–1.99 mm) for the same surfaces, confirming that δ and penetration depth are of the same millimetre order of magnitude. While local instantaneous penetration at individual asperities may exceed the averaged value, δ reflects the mean geometric interaction scale across the entire contact patch and therefore remains physically consistent with expected macro-texture penetration depths.

Table 4.1
Comparison of δ parameter and MPD under different pavement surface characteristics.

Type of the pavement	δ parameter (mm)	Mean MPD (mm)	Mean coefficient of rolling resistance (unitless)
DLPAC_0/5	0.11	0.89	0.00822
DLPAC_4/8	1.81	1.28	0.00869
New_PAC_16	1.44	1.68	0.00956
Worn_PAC_16	2.22	1.99	0.00977

4.2. Development of data-driven rolling resistance models

Commonly used data-driven models, MLR, RF, and ANN, were employed to predict the rolling resistance coefficient (RRC). The data collected from Phase I to Phase V were used for training and testing the models. The prediction accuracy of RRC was evaluated for all three models with and without considering the δ parameter. In order to simplify the complexity of the data-driven models, dimensionality reduction technique was applied using a correlation heat map and Exploratory Data Analysis (EDA).

4.2.1. Feature correlation analysis and dimensionality reduction

Fig. 4.1 illustrates the corresponding correlation heat map, where low colour intensity cells indicate no correlation, whereas high colour intensity cells indicate a strong positive or negative correlation between features in the dataset. It can be seen from Fig. 4.1 that the texture indicators ETD and RMS [10,25–27] exhibited a strong correlation with the MPD indicator with Pearson correlation coefficients of $r_{ETD} = 1$ and $r_{RMS} = 0.94$, respectively. A correlation coefficient of 1 indicates that the relationship assesses the same characteristic of pavement surface texture. In other words, MPD and ETD provide equivalent information about texture depth. Furthermore, the strong positive correlation of 0.94 between MPD and RMS suggests that an increase in MPD is typically accompanied by an increase in RMS, and vice versa. Consequently, the correlation values demonstrate that MPD, RMS, and ETD can reliably predict one another indicating that the three metrices functions equivalently in relation to surface texture. Therefore, MPD was chosen for developing ML models in this study, as it effectively represents RMS and ETD without significant loss of information.

As shown in Fig. 4.2, a feature importance analysis was conducted to evaluate the relative significance of the δ parameter in comparison to other features and rolling resistance presented in Fig. 4.1. The features MPD, ETD, RMS, the δ parameter, and Skewness were identified as the five most important features. Since the δ parameter is among the four leading features, it was also incorporated into the development of data-driven models. Temperature and pressure related features were not included in the analysis, as these measurements were maintained within narrow ranges (temperature: 22.44–28.72 °C; pressure: 205.2–212.6 kPa) with minimal variation during testing.

As discussed in Section 2, during the RR measurements, tire temperature, road temperature, and air temperature were continuously monitored. Within each measurement run, these variables were maintained approximately constant. The reported temperature range (22.44–28.72 °C) corresponds to differences between measurement days and pavement sections rather than intra-run fluctuations. Tire inflation pressure was actively controlled within a narrow band (205.2–212.6 kPa) with ±1 kPa precision. Exploratory analysis showed that RR variation across pavement sections was predominantly associated with texture-related features rather than with temperature drift within this range. Therefore, temperature and pressure effects were considered as controlled secondary variables within the present dataset. The influence of temperature and pressure on viscoelastic hysteresis behaviour is well

Fig. 4.1. Correlation heat map showing relationships among texture parameters, operational variables, the δ parameter, and RR coefficient (red = positive correlation; blue = negative correlation). Axis labels 1–10 correspond to: 1 = MPD, 2 = ETD, 3 = RMS, 4 = Skewness, 5 = Tire inflation pressure, 6 = Tire temperature, 7 = Road temperature, 8 = Air temperature, 9 = Delta parameter, and 10 = RR coefficient.

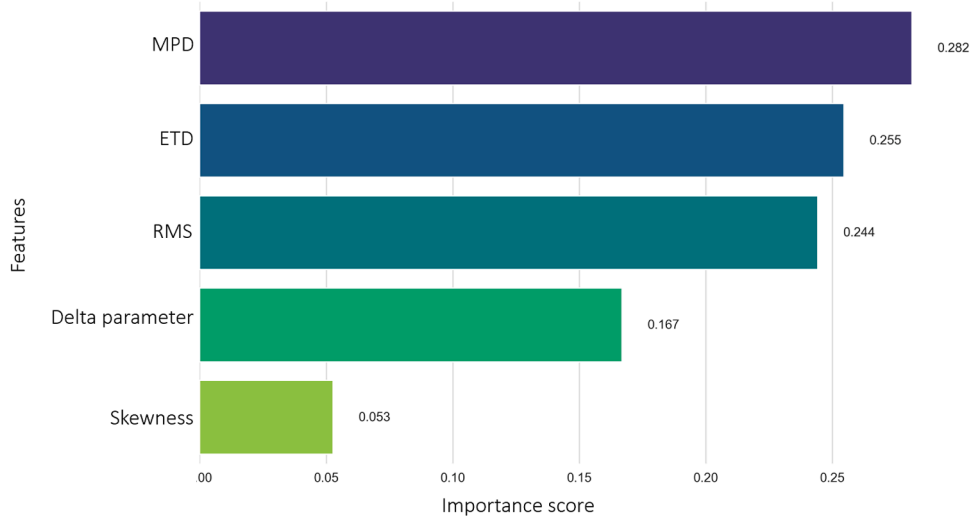

Fig. 4.2. Order of feature importances based on relative importance scores of input features for RRC prediction. MPD shows the highest contribution, followed by ETD and RMS, while the δ parameter provides moderate importance and skewness has the lowest influence.

established in the literature. Therefore, systematic evaluation under wider thermal and pressure operating ranges is recommended as an important direction for future research. Temperature and pressure-related features were nevertheless included in the feature correlation heat map for completeness.

Based on the outcomes from MPD, Skewness and the δ parameter and corresponding rolling resistance coefficients (RRC) were used to develop the data-driven models. The developed models were carefully evaluated and validated to ensure their robustness and reliability. The comprehensive evaluation process included checks for overfitting and underfitting as well as cross-validation and hyperparameter tuning. All of the efforts aimed at optimizing the models' performance and ensuring they generalize well to unseen data.

The dataset was randomly split into 70% training, 15% validation, and 15% testing sets for the development of the machine learning models. In order to prevent data leakage, feature normalization parameters (mean and standard deviation) were computed only from the training subset. The same statistics were then applied to validation and test sets. Target normalization was performed using training data statistics only. This ensures that no information from validation or test sets influenced model training. All samples belonging to the same pavement section were assigned to the same fold using a Group K-Fold strategy (K = 5). This approach ensures that model performance reflects generalization to unseen pavement sections rather than repeated measurements from the same section. Hyperparameter optimization of RF model was performed using randomized search within the training folds. The search space was defined as, Number of trees: 100–1200, Maximum tree depth: 5, 10, 15, 20, 25, 30, Maximum features per split: 'sqrt', Minimum samples to split: 2, 5, 10, 15, 100, Minimum samples per leaf: 1, 2, 5, 10. The ANN network architecture consisted of an input layer with three predictor variables, followed by two fully connected hidden layers comprising 12 and 16 neurons, respectively. A single neuron in the output layer was used to generate the final prediction. Rectified Linear Unit (ReLU) activation functions were applied to the hidden layers to

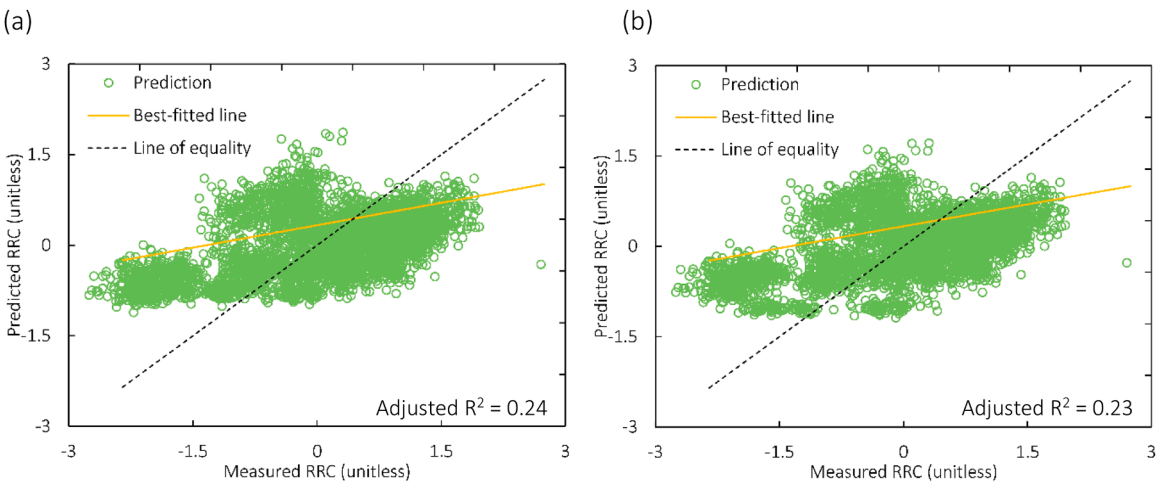

Fig. 4.3. Relationship between measured RRC and predicted RRC: (a) RRC prediction including δ parameter in the model[2] and, (b) RRC prediction excluding δ parameter in the model.

[2] Note that the values on the dependent and independent axes are presented after standardization.

Table 4.2
Performance of MLR model.

Performance metric	Including δ parameter	Excluding δ parameter
RMSE (mm)	0.000672	0.000674
MAE (mm)	0.000563	0.000565
Improvement of prediction	0.20 %	

Table 4.4
Performance of RF model.

Performance metric	Including δ parameter	Excluding δ parameter
RMSE (mm)	0.000573	0.000595
MAE (mm)	0.000451	0.000473
Improvement of prediction	3.52%	

Table 4.3
Comparison of RR prediction accuracy of MLR and commonly used LR models.

Equation of the model		Prediction accuracy (Adj. R^2)
$RRC = 0.68 \times MPD + 0.18 \times Skewness + 0.1 \times \delta$	(4.1) Fig. 4.3(a)	0.24
$RRC = 0.63 \times MPD + 0.2 \times Skewness$	(4.2) Fig. 4.3(b)	0.23
$RRC = 0.0009 \times MPD + 0.0078$	(4.3) [83]	0.22
$RRC = 0.0014 \times RMS + 0.0075$	(4.4) [83]	0.23
$RRC = 0.001 \times MPD + 0.0003 \times RMS + 0.0005 \times Skewness + 0.01$	(4.5) [83]	0.24
$RRC = 0.001 \times MPD + 0.0006 \times \left(\frac{MPD}{RMS}\right) + 0.0084$	(4.6) [83]	0.23

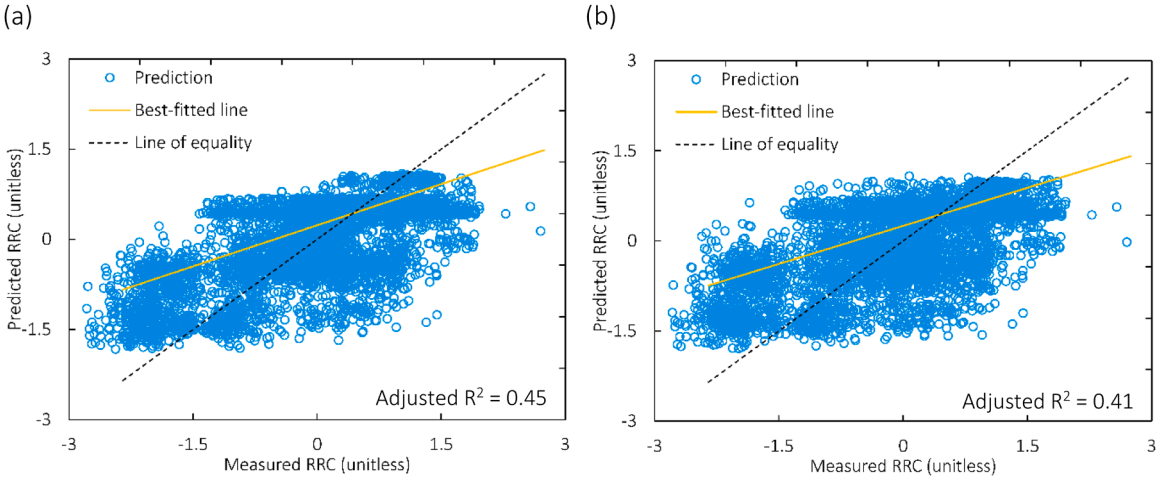

Fig. 4.4. Relationship between measured RRC and predicted RRC: (a) RRC prediction including δ parameter in the model[3] and, (b) RRC prediction excluding δ parameter in the model.

[3] Note that the values on the dependent and independent axes are presented after standardization.

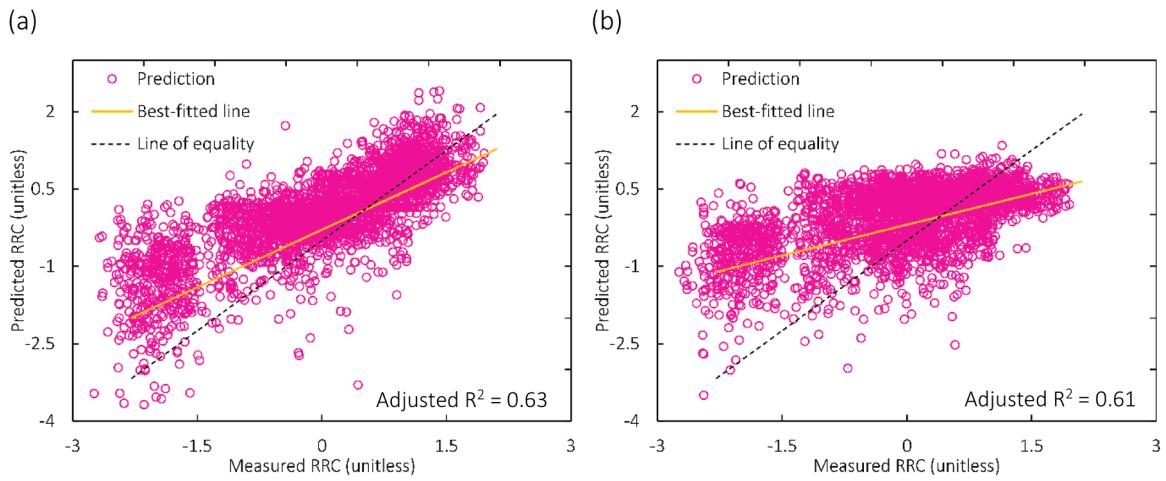

Fig. 4.5. Relationship between measured RRC and predicted RRC: (a) RRC prediction including δ parameter in the model[4] and, (b) RRC prediction excluding δ parameter in the model.

[4] Note that the values on the dependent and independent axes are presented after standardization.

introduce nonlinearity and improve convergence performance. To mitigate overfitting, a dropout layer with a dropout rate of 0.5 was incorporated during training. Additionally, L2 regularization (weight decay $= 5 \times 10^{-3}$) was applied to further constrain model complexity. Model optimization was performed using the Adam optimizer with a learning rate of 0.001. Early stopping based on validation loss was implemented to prevent overfitting and ensure generalization. To ensure full transparency and reproducibility, detailed cross-validation statistics, including fold-wise performance metrics and variance across repeated runs, are provided in Appendix.

4.2.2. *Influence of the δ parameter on prediction of rolling resistance using MLR model*

As shown in Fig. 4.3. the best-fitted and equality lines were plotted and the results were compared based on the prediction accuracy of RRC by including and excluding the δ parameter. It was found that the adjusted R^2 value excluding the δ parameter was 0.23, while the adjusted R^2 value including the δ parameter was 0.24. The parameter showed a positive effect on the model's explanatory power after the addition of the δ parameter.

Table 4.2, presents the performance of MLR model with and without the δ parameter. Performance metrices of root mean square error (RMSE) and mean absolute error (MAE) were used to assess the performance of the model. Based on the results, the percentage improvement in RMSE was 0.2%. In terms of RMSE, the δ parameter caused a slight improvement. Additionally, the δ parameter appeared to have a negligible but positive effect on the model by reducing the mean absolute error (MAE).

Table 4.3 presents the comparison of prediction accuracy between commonly used linear and multiple linear regression models and the ML-based models as shown in Fig. 4.3. The prediction accuracies were all below or equal to an Adjusted R^2 of 0.24, indicating a poor level of prediction. The results indicated that the LR and MLR models were not capable of capturing the complexity of the relationships between the selected features, and RRC effectively. Hence, it can be concluded that the LR and MLR models unable to capture the non-linear behavior between the features and the target variable (RRC) [6]. The results suggest the need for a more complex model such as ensemble learning method or neural networks to capture non-linear relationships more effectively.

4.2.3. *Influence of the δ parameter on prediction of rolling resistance using RF model*

Results of the RF model are illustrated in Fig. 4.4. The results were compared based on the prediction accuracy of RRC by including and excluding the δ parameter. The adjusted R^2 including δ parameter (see Fig. 4.4(a)) was 0.45. The adjusted R^2 excluding δ parameter (see Fig. 4.4(b)) was 0. 41. As indicated by the increase in adjusted R^2, the δ parameter has a greater positive effect on the explanatory power of the RF model compared to the MLR model. The prediction of RRC improved by 3.5% with the addition of the δ parameter to the model.

As given in Table 4.4, the percentage improvement in RMSE was 3.5%. In terms of RMSE, the δ parameter resulted a noticeable improvement compared to MLR model. Additionally, the δ parameter had a minimal but positive impact on the model by lowering the MAE (Tables 1.1 and 1.2).

4.2.4. *Influence of the δ parameter on prediction of rolling resistance using ANN model*

Fig. 4.5 presents the relationship between measured RRC and predicted RRC using ANN model. The adjusted R^2 including δ parameter (see Fig. 4.5(a)) was 0.63. The adjusted R^2 excluding δ parameter (see Fig. 4.5(b)) was 0. 61. The improvement of the prediction accuracy after adding the δ parameter to the model was 3.7%. As indicated by the increase in adjusted R^2, the δ parameter has an improved positive effect on the explanatory power of the ANN model compared to both RF and MLR models.

As given in Table 4.5, the percentage improvement in RMSE was 3.7%. In terms of RMSE, the δ parameter resulted an improvement in prediction accuracy compared to both RF and MLR model. Additionally, the δ parameter had a minimal but positive impact on the model by lowering the MAE (Tables 1.3 and 1.4).

Table 4.5
Performance of ANN model.

Performance metric	Including δ parameter	Excluding δ parameter
RMSE (mm)	0.000469	0.000487
MAE (mm)	0.000357	0.000369
Improvement of prediction	3.70%	

Table 4.6
RR prediction accuracy under different prediction models.

Rolling resistance prediction model	Expression of the model	Features in the model including δ parameter	Model accuracy – Adj. R^2	Features in the model excluding δ parameter	Model accuracy - Adj. R^2	Prediction accuracy improvement with δ parameter (%)
MLR - proposed	(4.1) and (4.2)	MPD, Skewness, δ parameter	0.24	MPD, Skewness, δ parameter	0.23	0.20
[83]	(4.3)	-	-	MPD	0.22	-
[83]	(4.4)	-	-	MPD, RMS	0.23	-
[83]	(4.5)	-	-	MPD, RMS, Skewness	0.24	-
[83]	(4.6)	-	-	MPD, RMS	0.23	-
RF - proposed	-	MPD, Skewness, δ parameter	0.45	MPD, Skewness, δ parameter	0.41	3.52
ANN - proposed	-	MPD, Skewness, δ parameter	0.63	MPD, Skewness, δ parameter	0.61	3.70

4.3. Comparison of rolling resistance prediction models and the effect of the δ parameter

Table 4.6 presents a summary of different RR prediction models and comparison of their prediction capabilities. The ANN - proposed and RF - proposed models provided better predictions of RR compared to the other models listed in Table 4.6. As compared to the models from (4.3) to (4.6), the prediction accuracy showed a slight improvement with the inclusion of the physics-based feature, the δ parameter, in the RF - proposed and ANN - proposed models. Regardless of the R^2 value, the inclusion of the δ parameter feature in the ML models enhanced prediction accuracy. This suggests that incorporating additional data, including the δ parameter, into the system has the potential to further improve RRC prediction. The primary reasons for the lower Adj. R^2 could include the inadequate the low resolution of the available LCMS data, and the limited data availability. Although the inclusion of the δ parameter resulted in statistically significant improvements across all models, the absolute increase in adjusted R^2 values was modest for MLR model. This indicates that δ does not substantially alter linear relationships but contributes additional explanatory power when nonlinear interactions are considered.

Fig. 4.6 shows the influence of Skewness, MPD, and the δ parameter on RRC prediction across the three developed models. Best-fit lines were plotted for three approaches, the reference model (considering only Skewness), the traditional model (considering both MPD and Skewness), the proposed model (considering MPD, Skewness, and the δ parameter), and the models' accuracies were compared against the line of equality. The parameter Skewness was incorporated into the reference model to assess the benefits of including the MPD and δ parameter together with Skewness for enhancing the prediction accuracy of RR. The analysis showed that the reference model exhibited the greatest deviation from the line of equality, as indicated by the largest angle. In contrast, the smallest angle with the line of equality was observed in the proposed model.

Among all models, the ANN model demonstrated the smallest angle and the highest predictive accuracy relative to the line of equality by incorporating all three states. The traditional model showed a slight improvement in RRC prediction compared to the reference models but performed lower than the proposed models. Based on the results, it can be concluded that the inclusion of the δ parameter enhances RRC prediction performance without compromising accuracy. It is noted that this study utilized a limited trial section dataset for the δ parameter. Incorporating more data of the δ parameter is expected to enhance the prediction accuracy of RR.

4.4. Reliability assessment of δ parameter

Statistical methods were employed to assess the reliability of the δ parameter as an indicator for replacing direct measurements of tire-pavement interaction. The predicted RRC values from the RF-proposed and ANN-proposed models were considered in the statistical analysis because these two models had been identified in earlier analyses of the study as the best-performing. In order to completely be unbiased, the analysis was exposed to measured and predicted sources of RRC data. For the predicted RRC data, the statistical analysis utilized values from both models with and without the inclusion of the δ parameter. As recommended by statisticians [93–96] examining a normality of the data aids determine the appropriate type of further analysis to perform. Therefore, Anderson-Darling (AD) test [93,94,96] was conducted to assess whether the data followed a normal distribution. The null hypothesis (H_0) assumes that the data are normally distributed, while the alternative hypothesis (H_1) suggests that the data are not normally distributed. As given in Table 4.7, the Test Statistic (AD) was observed to be significantly higher than the corresponding critical values for all datasets from both models. Therefore, the null hypothesis was rejected, indicating that the data do not follow a normal distribution. This non-normal distribution indicates the complex and nonlinear interactions inherent in rolling resistance phenomena. Factors such as tire deformation, surface roughness, and material heterogeneity, etc. introduce variability and asymmetry into the RR measurements. As a result, the distributions are skewed or have heavy tails instead of being symmetric. Many past studies have overlooked this asymmetry in RRC data, often assuming a normal distribution and applying traditional statistical analyses. Under this assumption, these studies typically explored relationships between RRC and both tire and pavement related parameters using R^2 as the primary metric, considering it the most appropriate approach. The findings of the present study, indicate that the RRC data in the present dataset deviate from strict normality. This behaviour is not unexpected, as rolling resistance values are typically bounded and influenced by multiple interacting physical factors, which may introduce skewness or mild asymmetry. The purpose of conducting the AD test was not to challenge prior studies, but to assess the distributional characteristics of the current dataset. It is noted that the AD test was conducted separately for each model using the corresponding cross-validation folds. Therefore, the reported AD statistics for the measured RRC differ between the RF and ANN models due to differences in fold composition and sample distribution. Based on the observed deviation from normality, a non-parametric paired test (Wilcoxon signed-rank test) was selected to conservatively evaluate whether inclusion of the δ parameter significantly reduces prediction error. This approach complements conventional parametric metrics such as R^2, RMSE, and MAE by providing distribution-robust statistical validation.

As given in Table 4.7, the results from the AD test showed that the data deviate from a normal distribution, making parametric methods unsuitable for proper analysis. This is because the mean is heavily influenced by skewness or outliers and may not provide a reliable measure of central tendency under such conditions. In contrast, the median is more robust in these cases. RRC predictions can exhibit occasional extreme values due to irregularities in tire-pavement interactions, abrupt environmental variations, and other factors. Under extreme conditions these irregularities can distort the mean but have minimal impact on the median. Therefore, the Wilcoxon signed-rank test

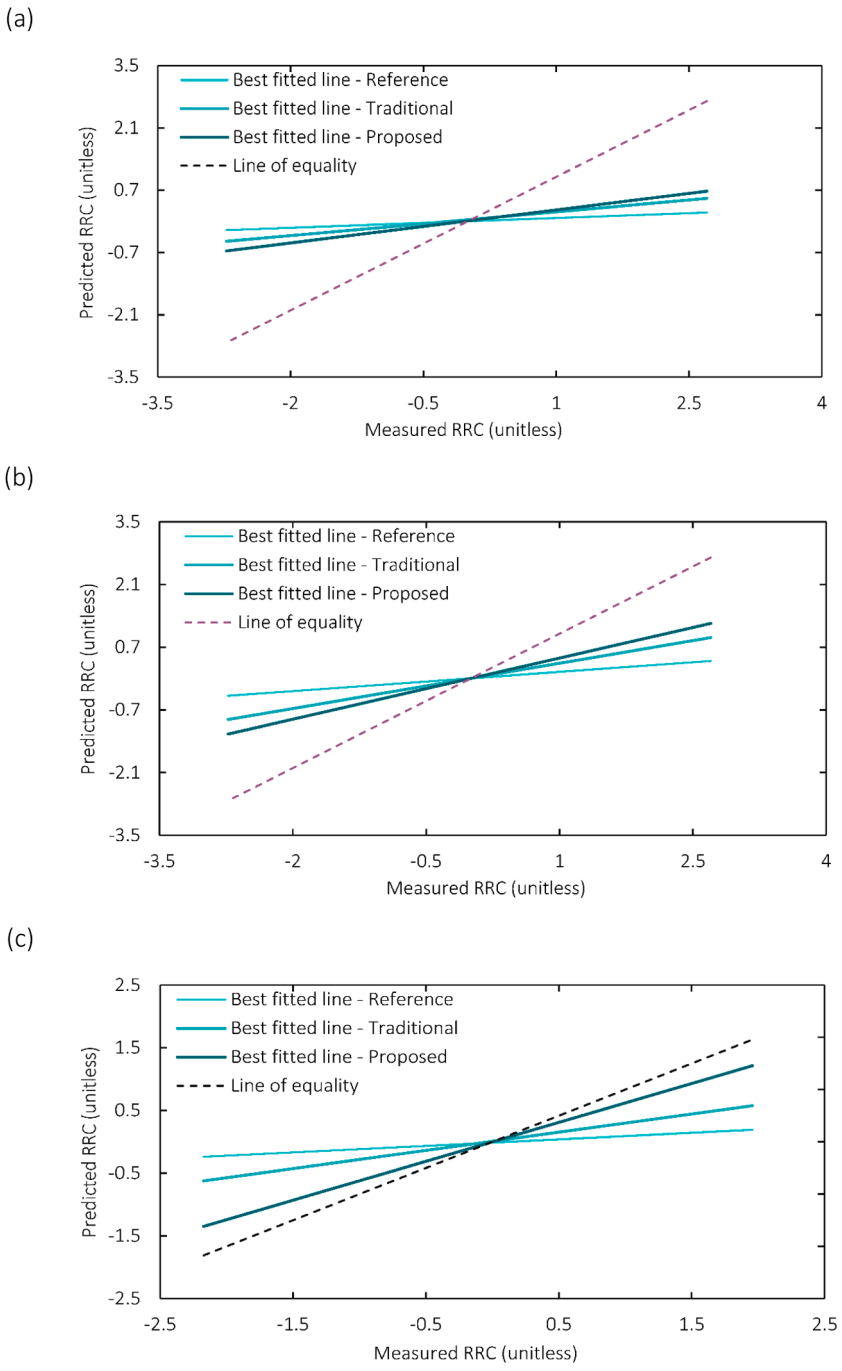

Fig. 4.6. Influence of the δ parameter on RRC prediction compared to traditional parameters: (a) MLR model, (b) RF model and, (c) ANN model.[5] The dashed line indicates perfect agreement (y = x). The solid lines show best-fit trends for models with and without the δ parameter.

[5] Note that the values on the dependent and independent axes are presented after standardization.

Table 4.7
Anderson-Darling (AD) test.

Model	Dataset	Test Statistic (AD)	Critical value			Status of hypothesis
			significance level: 1%	significance level: 5%	significance level: 10%	
RF	Measured RRC	79.826	1.091	0.786	0.655	Reject H_0
	Predicted RRC – Including δ parameter	230.240				
	Predicted RRC – Excluding δ parameter	224.258				
ANN	Measured RRC	44.679				
	Predicted RRC – Including δ parameter	62.264				
	Predicted RRC – Excluding δ parameter	35.705				

Table 4.8
Wilcoxon signed-rank test.

Model	Significance level	p-value	Status of hypothesis
RF	5%	4.767×10^{-25}	Reject H_0
ANN	5%	0.007	Reject H_0

[97–99] was selected for this analysis, as it is a robust non-parametric method suitable for paired data that do not follow a normal distribution. Moreover, the Wilcoxon signed-rank test specifically evaluates whether the median of the differences between paired observations differs from zero, making it appropriate for assessing the effect of the δ parameter on reducing the model's prediction error. Accordingly, the null hypothesis (H_0) assumes that the δ parameter has no significant influence on the reduction of the model's prediction error, while the alternative hypothesis (H_1) assumes that the δ parameter significantly reduces the prediction error.

The results in Table 4.8 indicate that the Wilcoxon signed-rank test confirms the effectiveness of incorporating the δ parameter in reducing prediction errors. For the RF model, the p-value was found to be 4.767×10^{-25}, which is far below the conventional significance level of 0.05. This extremely low p-value provides strong evidence to reject the null hypothesis (H_0), indicating that the absolute error of RRC with the δ parameter is significantly lower than without δ parameter. In other words, including the δ parameter leads to a substantial improvement in the model's prediction accuracy. Similarly, ANN model yielded a p-value of 0.007, which is also below 0.05. This result confirms that the reduction in absolute error of RRC observed when adding the δ parameter is statistically significant for the ANN model as well. Therefore, for both RF and ANN models, there seems to be consistent and compelling evidence that the δ parameter plays a meaningful role in enhancing predictive performance by effectively lowering the prediction error. These findings underscore the importance of incorporating the δ parameter in RRC prediction models. In addition to adjusted R^2 (Table 4.4 and Table 4.5), model performance was evaluated using RMSE and MAE to assess practical error reduction. For the RF model, inclusion of δ reduced RMSE from 0.000595 to 0.000573 (3.52% improvement), while for the ANN model RMSE decreased from 0.000487 to 0.000469 (3.70% improvement). Although these reductions may appear numerically small, they represent consistent improvements across the entire dataset and were confirmed statistically using the Wilcoxon signed-rank test. Accounting for the factors captured by δ parameter, both machine learning models demonstrate improved robustness and reliability, particularly in handling the complexities and nonlinearities inherent to tire-pavement interactions.

5. Conclusions

This research focused on improving the prediction of RR by introducing a parameter related to tire-pavement interaction into RR prediction models. The primary objective of this study was to develop a framework that integrates both data-driven and physics-based approaches to enhance the prediction of rolling resistance. The study investigated the relationships between rolling resistance, a physics-based parameter known as the δ parameter, and texture properties. To develop the proposed framework, machine learning (ML) models were employed, including MLR, RFR, and ANN. The improved RR predictions were evaluated by incorporating the δ parameter within the data-driven models. The significant impact of the δ parameter on model performance was evaluated using the statistical non-parametric Wilcoxon signed-rank test.

The analysis of the texture pad-based δ parameter under static loading conditions confirmed that the FEM tire-pavement interaction model aligns with field-measured experimental δ parameters at an acceptable level. The model demonstrated similar tire-penetration patterns and penetration depths, thereby validating its accuracy in simulating in-field conditions. The validation accuracy of the FEM model was observed as MAPE of 7.19%.

The EDA analysis demonstrated a strong correlation between MPD, ETD, and RMS, confirming that the metrices provide equivalent insights into surface texture. Feature importance analysis highlighted the MPD and δ parameter as a crucial factor in tire-surface interactions. Based on the analysis it was found that the δ parameter plays a localized role in rolling resistance. Skewness had minimal influence, reinforcing its statistical rather than mechanical significance. MPD, Skewness, and the δ parameter were integrated into data-driven models to ensure accurate and reliable predictions of rolling resistance.

The comparison of MPD and δ parameter across four different pavement surfaces highlighted the influence of aggregate size on surface texture and roughness. The DLPAC_0/5 pavement exhibited the lowest values by indicating a smooth surface with minimal rolling resistance. In contrast, the DLPAC_4/8, New_PAC_16 and Worn_PAC_16 pavements indicated increased roughness, with Worn_PAC_16 showing the highest values due to wear and damages. The findings suggest that larger aggregate sizes contribute to higher MPD and δ parameter values. Which significantly affects tire-pavement interactions and increasing the rolling resistance.

The comparison of different regression and machine learning models highlighted the limitations of linear models (LR and MLR) in capturing the complex relationships between surface texture and rolling resistance. The inclusion of the δ parameter had a positive impact on model performance. The ML models, ANN and RF, demonstrated notably better predictive capabilities with the inclusion of δ parameter compared to LR and MLR models. The δ parameter contributed more significantly to the performance of the RF and ANN models than to the MLR model, emphasizing its role in nonlinear modeling. It is important to note that the inclusion of the δ parameter did not lead to a substantial increase in prediction accuracy in absolute terms. Rather, its primary contribution lies in introducing a physics-based descriptor of tire-pavement interaction into the data-driven modeling framework. The improvement was more pronounced in nonlinear models (RF and ANN), indicating that δ interacts with texture parameters in a nonlinear manner. Therefore, the practical significance of δ should be interpreted as enhancing model robustness and physical interpretability, rather than serving as a single dominant predictor of rolling resistance. Furthermore, the primary contribution of this study lies in demonstrating the feasibility of integrating the δ parameter into data-driven rolling resistance prediction models, rather than in establishing the absolute superiority of any particular machine learning algorithm.

The Wilcoxon signed-rank test showed strong statistical evidence that incorporating the δ parameter significantly reduces the prediction error in both RF and ANN models, hence improves rolling resistance predictions. This finding highlights that non-parametric statistical testing can provide additional robustness when evaluating improvements in prediction error under datasets that deviate from strict normality.

6. Future research directions

This study demonstrates significant advancements in predicting rolling resistance by integrating δ parameters with data-driven models. The study also establishes a foundation for future investigations that could ultimately lead to practical advancements in real-time prediction of rolling resistance and improvements in pavement design strategies. However, there are several directions for further improvement and practical application. Expanding the dataset to include a broader range of pavement types and test conditions will enhance the models' robustness and real-world applicability. Field validation is essential for expanding the dataset. Therefore, upgrading the developed portable device by incorporating standard reference testing tires (SRTT) at real size could yield more accurate δ parameter data. Therefore, experimental validation of the δ parameter using a full-scale SRTT tire under

controlled field conditions is acknowledged as an important direction for future research. Future work should also focus on refining machine learning models, exploring advanced techniques, and optimizing performance for improved accuracy. Further studies should test the models under a variety of traffic conditions, vehicle speeds, tire types, and environmental factors to evaluate their practical applicability.

Data availability

The data used in this study is not publicly available due to the inclusion of sensitive or confidential information, in accordance with the agreement made with the relevant authority.

CRediT authorship contribution statement

W.A.A.S. Premarathna: Writing – review & editing, Writing – original draft, Visualization, Validation, Resources, Methodology, Investigation, Formal analysis, Data curation. **Kumar Anupam:** Writing – review & editing, Writing – original draft, Validation, Supervision, Resources, Project administration, Methodology, Investigation, Funding acquisition, Conceptualization. **M. Moenielal:** Writing – review & editing, Resources, Project administration, Investigation, Data curation. **Thijs Wensveen:** Writing – review & editing, Resources, Data curation. **Cor Kasbergen:** Writing – review & editing, Supervision, Software, Resources, Project administration. **Sandra M.J.G. Erkens:** Writing – review & editing, Supervision, Project administration, Investigation.

Declaration of competing interest

The authors declare the following financial interests/personal relationships which may be considered as potential competing interests: Kumar Anupam reports financial support was provided by Rijkswaterstaat (RWS). If there are other authors, they declare that they have no known competing financial interests or personal relationships that could have appeared to influence the work reported in this paper.

Acknowledgment

The authors gratefully acknowledge the support received from the Knowledge-based Pavement Engineering (KPE) research program. KPE is a collaborative initiative involving Rijkswaterstaat, TNO, and TU Delft, aimed at advancing scientific and applied knowledge in the field of asphalt pavements. This research contributes to Rijkswaterstaat's ambitious objectives of achieving complete climate neutrality and embracing circular principles by 2030.

Appendix

1. Hyperparameter convergence and stability analysis of Random Forest and Artificial Neural Network models

Table 1.1
Convergence and stability analysis of RF model including δ.

Iter	CV R^2	Test R^2	Test RMSE	Test MAE	Std Across Runs
1	0.42±0.03	0.43 ± 0.04	0.000610±0.000025	0.000480±0.000020	0.05
5	0.44± 0.025	0.445± 0.03	0.000590±0.000020	0.000465±0.000017	0.03
10	0.445±0.020	0.450±0.025	0.000582±0.000018	0.000458±0.000015	0.022
20	0.448±0.018	0.453±0.020	0.000577±0.000015	0.000454±0.000013	0.015
30	0.450±0.015	0.455±0.018	0.000575±0.000013	0.000452±0.000012	0.013
40	0.452±0.013	0.456±0.016	0.000574±0.000012	0.000451±0.000011	0.012
50	0.453±0.012	0.457±0.015	0.000573±0.000010	0.000451±0.000009	0.012

Table 1.2
Convergence and stability analysis of RF model excluding δ.

Iter	CV R^2	Test R^2	Test RMSE	Test MAE	Std Across Runs
1	0.40±0.035	0.41±0.04	0.000630±0.000030	0.000500±0.000025	0.055
5	0.42±0.028	0.43±0.03	0.000610±0.000025	0.000485±0.000020	0.035
10	0.425±0.022	0.435±0.025	0.000602±0.000020	0.000478±0.000017	0.025
20	0.430±0.018	0.440±0.020	0.000598±0.000017	0.000475±0.000015	0.017
30	0.432±0.016	0.442±0.018	0.000596±0.000015	0.000474±0.000013	0.014
40	0.433±0.014	0.443±0.017	0.000595±0.000013	0.000473±0.000012	0.012
50	0.434±0.013	0.444±0.015	0.000595±0.000012	0.000473±0.000010	0.012

Table 1.3
Convergence and stability analysis of ANN model including δ.

Epochs	CV R^2 (mean ± std)	Test R^2 (mean ± std)	Test RMSE (mean ± std)	Test MAE (mean ± std)	Std Across Runs (R^2)
100	0.56±0.03	0.55±0.04	0.000520±0.000020	0.000395±0.000018	0.05
200	0.59±0.025	0.58±0.035	0.000505±0.000018	0.000385±0.000016	0.04
500	0.61±0.020	0.60±0.030	0.000490±0.000015	0.000372±0.000014	0.03
1000	0.62±0.018	0.61±0.025	0.000478±0.000012	0.000365±0.000012	0.022
1500	0.625±0.016	0.613±0.022	0.000474±0.000010	0.000362±0.000011	0.018
2000	0.632±0.015	0.615±0.020	0.000471±0.000009	0.000359±0.000010	0.016
2500	0.638±0.014	0.617±0.018	0.000469±0.000008	0.000357±0.000009	0.015

Table 1.4
Convergence and stability analysis of ANN model excluding δ.

Epochs	CV R^2 (mean ± std)	Test R^2 (mean ± std)	Test RMSE (mean ± std)	Test MAE (mean ± std)	Std Across Runs (R^2)
100	0.54±0.03	0.53±0.04	0.000540±0.000022	0.000410±0.000020	0.055
200	0.57±0.025	0.56±0.035	0.000525±0.000019	0.000400±0.000017	0.045
500	0.59±0.020	0.58±0.030	0.000508±0.000016	0.000387±0.000015	0.033
1000	0.60±0.018	0.595±0.025	0.000498±0.000013	0.000379±0.000013	0.024
1500	0.605±0.016	0.600±0.022	0.000494±0.000011	0.000375±0.000012	0.02
2000	0.610±0.015	0.603±0.020	0.000490±0.000010	0.000372±0.000011	0.017
2500	0.615±0.014	0.605±0.018	0.000487±0.000009	0.000369±0.000010	0.016

References

[1] J. Feng, C. Sandu, V. Tech, T. Li, and R. Burdisso, "The effects of tread pattern on tire pavement interaction noise," 2016. [Online]. Available: https://www.researchgate.net/publication/338374952.

[2] Mahajan GR, Radhika B, Biligiri KP. A critical review of vehicle-pavement interaction mechanism in evaluating flexible pavement performance characteristics. Road Mater Pavement Des 2022;23(4):735–69. https://doi.org/10.1080/14680629.2020.1860806.

[3] Gong Z, Miao Y, Lantieri C. Review of research on tire–pavement contact behavior. Multidisciplinary Digital Publishing Institute (MDPI); Feb. 01, 2024. https://doi.org/10.3390/coatings14020157.

[4] Liu Q, et al. Analysis of tire-pavement interaction modeling and rolling energy consumption based on finite element simulation. Constr Build Mater Apr. 2024;425. https://doi.org/10.1016/j.conbuildmat.2024.136101.

[5] Spies L, Li T, Burdisso R, Sandu C. An artificial neural network (ANN) approach to model tire-pavement interaction noise (TPIN) based on tire noise separation. Appl Acoust Apr. 2023;206. https://doi.org/10.1016/j.apacoust.2023.109294.

[6] Araújo JPC, Palha CAO, Martins FF, Silva HMRD, Oliveira JRM. Estimation of energy consumption on the tire-pavement interaction for asphalt mixtures with different surface properties using data mining techniques. Transp Res D Transp Environ Feb. 2019;67:421–32. https://doi.org/10.1016/j.trd.2018.12.022.

[7] K. Gopalakrishnan, J. Steyn, and J. Harvey, "Green energy and Technology Climate change, energy, sustainability and pavements," 2014. [Online]. Available: http://www.springer.com/series/8059.

[8] He Y, et al. Study on the influence of tire polishing on surface texture durability and skid resistance deterioration of asphalt pavement. Wear Nov. 2024;556–557. https://doi.org/10.1016/j.wear.2024.205518.

[9] Yu M, et al. Skid resistance in pavement-vehicle interaction with anti-lock braking systems. Int J Pavement Eng 2024;25(1). https://doi.org/10.1080/10298436.2024.2380514.

[10] Ejsmont JA, Ronowski G, Świeczko-Żurek B, Sommer S. Road texture influence on tyre rolling resistance. Road Mater Pavement Des Jan. 2017;18(1):181–98. https://doi.org/10.1080/14680629.2016.1160835.

[11] Romero CA, Correa P, Ariza Echeverri EA, Vergara D. Strategies for reducing automobile fuel consumption. Multidisciplinary Digital Publishing Institute (MDPI); Jan. 01, 2024. https://doi.org/10.3390/app14020910.

[12] Jiang R, Wu P, Wu C. Driving factors behind energy-related carbon emissions in the U.S. Road transport sector: a decomposition analysis. Int J Env Res Public Health Feb. 2022;19(4). https://doi.org/10.3390/ijerph19042321.

[13] Sun Z, Premarathna WAAS, Anupam K, Kasbergen C, Erkens SMJG. A state-of-the-art review on rolling resistance of asphalt pavements and its environmental impact. Elsevier Ltd; Jan. 12, 2024. https://doi.org/10.1016/j.conbuildmat.2023.133589.

[14] Chun J, McKeown J, Kang S. Impact of vehicle electrification on road roughness induced greenhouse gas (GHG) emissions. Sustain Energy Technol Assess Apr. 2024;64. https://doi.org/10.1016/j.seta.2024.103701.

[15] Ejsmont J, Sommer S. Selected aspects of pavement texture influence on tire rolling resistance. Coatings Jul. 2021;11(7). https://doi.org/10.3390/coatings11070776.

[16] Ding S, Wang KCP, Yang E, Zhan Y. Influence of effective texture depth on pavement friction based on 3D texture area. Constr Build Mater 2021;287:123002. https://doi.org/10.1016/j.conbuildmat.2021.123002.

[17] D. Yun, C. Tang, U. Sandberg, L. Hu, A. Sha, and M. Ran, "A new method to measure rubber penetration depth for pavements to better predict the tire-road friction coefficient acknowledgement A new method to measure rubber penetration depth for," 2022.

[18] Ejsmont J, Owczarzak W. Engineering method of tire rolling resistance evaluation. Measurement 2019;145:144–9. https://doi.org/10.1016/j.measurement.2019.05.071.

[19] Shakiba M, Ozer H, Ziyadi M, Al-Qadi IL. Mechanics based model for predicting structure-induced rolling resistance (SRR) of the tire-pavement system. Mech Time Depend Mater Nov. 2016;20(4):579–600. https://doi.org/10.1007/s11043-016-9313-0.

[20] Ronowski G. Design and calibration of rolling resistance test trailer R2Mk.2. In: IOP Conference Series: Materials Science and Engineering. Institute of Physics Publishing; Sep. 2016. https://doi.org/10.1088/1757-899X/148/1/012026.

[21] Ejsmont J, Ronowski G, Ydrefors L, Owczarzak W, Sommer S, Świeczko-Żurek B. Comparison of tire rolling resistance measuring methods for different surfaces. Int J Automot Technol 2024;25(4):965–76. https://doi.org/10.1007/s12239-024-00092-w.

[22] Ydrefors L, Hjort M, Kharrazi S, Jerrelind J, Stensson Trigell A. Rolling resistance and its relation to operating conditions: a literature review. SAGE Publications Ltd; Oct. 01, 2021. https://doi.org/10.1177/09544070211011089.

[23] ŚWIECZKO-ŻUREK B, RONOWSKI G, EJSMONT J. Tyre rolling resistance and its influence on fuel consumption. Combust Engines Feb. 2017;168(1):62–7. https://doi.org/10.19206/ce-2017-110.

[24] S. Rajaei and K. Chatti, "Mechanistic modeling of the effect of pavement surface profile on rolling resistance final project report," 2020. [Online]. Available: http://www.chpp.egr.msu.edu/.

[25] M. Haider, M. Conter, R. Wehr, U. Sandberg,; Reinhard Wehr, and; Fabienne Anfosso, "Project ROSANNE: rolling resistance, skid resistance, and noise emission measurement standards for road surfaces," 2014. [Online]. Available: https://hal.science/hal-01470451v1.

[26] U. Sandberg, J.A. Ejsmont, A. Bergiers, L. Goubert, M. Zöller, and R. Karlsson, "Road surface influence on tyre/road rolling resistance," 2011. [Online]. Available: http://www.miriam-co2.net/.

[27] U. Sandberg, A. Bergiers, J.A. Ejsmont, L. Goubert, and M. Zöller, "Rolling resistance – Measurement methods for studies of road surface effects," 2012. [Online]. Available: http://www.miriam-co2.net/.

[28] Boere S, Arteaga ILopez, Kuijpers A, Nijmeijer H. Tyre/road interaction model for the prediction of road texture influence on rolling resistance. Int J Veh Des 2014;65(2–3):202–21. https://doi.org/10.1504/IJVD.2014.060815.

[29] Kane M, Riahi E, Do MT. Tire/road rolling resistance modeling: discussing the surface macrotexture effect. Coatings 2021;11(5). https://doi.org/10.3390/coatings11050538.

[30] Riahi E, Ropert C, Do MT. Developing a laboratory test method for rolling resistance characterisation of road surface texture. Surf Topogr 2020;8(2). https://doi.org/10.1088/2051-672X/ab8aa6.

[31] S. Boere, I. Lopez, A.H.W.M. Kuijpers, and H. Nijmeijer, "Tyre/road interaction model for the prediction of rolling resistance of due to texture induced tyre vibrations," 2009.

[32] Garcia MA, Israfilova A, Liang G, Zhao T, Wei Y, Kaliske M. Isogeometric analysis for accurate modeling of rolling tires. Comput Struct Feb. 2022;260. https://doi.org/10.1016/j.compstruc.2021.106717.

[33] Wang D, Ueckermann A, Schacht A, Oeser M, Steinauer B, Persson BNJ. Tire-road contact stiffness. Tribol Lett 2014;56(2):397–402. https://doi.org/10.1007/s11249-014-0417-x.

[34] Persson BNJ. Theory of rubber friction and contact mechanics. J Chem Phys Aug. 2001;115(8):3840–61. https://doi.org/10.1063/1.1388626.

[35] Yang C, Persson BNJ. Contact mechanics: contact area and interfacial separation from small contact to full contact. J Phys Condens Matter 2008;20(21). https://doi.org/10.1088/0953-8984/20/21/215214.

[36] Almqvist A, Campañá C, Prodanov N, Persson BNJ. Interfacial separation between elastic solids with randomly rough surfaces: comparison between theory and numerical techniques. J Mech Phys Solids Nov. 2011;59(11):2355–69. https://doi.org/10.1016/j.jmps.2011.08.004.

[37] Yun D, et al. A new approach for determining rubber enveloping on pavement and its implications for friction estimation. Coatings Mar. 2024;14(3). https://doi.org/10.3390/coatings14030301.

[38] Zhou H, Hu Z, Gao Z, Li H, Xiao S. An evaluation method for penetration depth of rubber on rough surface and analysis of influencing factors. Tribol Lett 2025;73(4):148. https://doi.org/10.1007/s11249-025-02085-x.

[39] Ejsmont J, Sommer S. Selected aspects of pavement texture influence on tire rolling resistance. Coatings Jul. 2021;11(7). https://doi.org/10.3390/coatings11070776.

[40] Hashmi AW, Mali HS, Meena A, Hashmi MF, Bokde ND. Surface characteristics measurement using computer vision: a review. Tech Science Press; 2023. https://doi.org/10.32604/cmes.2023.021223.

[41] N. Nithyanantham and P. Suresh, "Evaluation of cast iron surface roughness using image processing and machine vision system," vol. 11, no. 2, 2016, [Online]. Available: www.arpnjournals.com.

[42] A.C. Reddy, "Evaluation of surface roughness using a image processing and machine vision system," 2004.

[43] Fahad M. Optimization of pavement texture depth measurement using machine learning algorithms. Discov Appl Sci 2026. https://doi.org/10.1007/s42452-026-08392-9.

[44] Fakhri M, Pourjafar SV, Daneshvari MH. Texture-based image analysis and explainable machine learning for polished asphalt identification in pavement

condition monitoring. Sci Rep 2025;15(1):43167. https://doi.org/10.1038/s41598-025-27203-6.
[45] Song H, LEE DH, Chung H. Development of prediction model for vehicle road load using machine learning. SAE technical paper. 2025.
[46] Yadav R, Raheman H. A machine learning-based approach for estimation of deflection and contact area characteristics of tubeless and tube-type agricultural tyres. Eng Appl Artif Intell Jul. 2024;133. https://doi.org/10.1016/j.engappai.2024.108357.
[47] Chen F, Luo Z, Ma T, Chen S. Estimation of the pavement skid resistance by automated vehicle based on one-dimensional convolutional neural network. Int J Pavement Eng 2024;25(1). https://doi.org/10.1080/10298436.2024.2343086.
[48] Uva I, Santos J, Cerezo V, Miller S. A machine learning approach for predictive modelling of rolling resistance of passenger cars. Int J Pavement Eng Dec. 2025;26(1):2553717. https://doi.org/10.1080/10298436.2025.2553717.
[49] Zeiada W, Alnaqbi A, Al-Khateeb GG, Abuzwidah M. Towards safer roads: machine learning models for predicting pavement friction in CRCP. J Umm Al-Qura Univ Eng Archit 2025. https://doi.org/10.1007/s43995-025-00263-5.
[50] Demetgul M, Lazarova-Molnar S. Data-driven artificial intelligence applications for tyre-road-noise prediction and road condition monitoring: a review and future directions. Measurement 2026;264:120203. https://doi.org/10.1016/j.measurement.2025.120203.
[51] Yadav R, Raheman H. A machine learning-based approach for estimation of deflection and contact area characteristics of tubeless and tube-type agricultural tyres. Eng Appl Artif Intell 2024;133:108357. https://doi.org/10.1016/j.engappai.2024.108357.
[52] Koné A, Es-Sabar A, Do M-T. Application of machine learning models to the analysis of skid resistance data. Lubricants 2023;11(8). https://doi.org/10.3390/lubricants11080328.
[53] Zhong J, et al. Texture-image coupled fusion analysis for pavement skid resistance measurement. Measurement 2025;256:118272. https://doi.org/10.1016/j.measurement.2025.118272.
[54] B.N.J. Persson, "On the theory of rubber friction," 1998.
[55] B.N.J. Persson, O. Albohr, U. Tartaglino, A.I. Volokitin, and E. Tosatti, "On the nature of surface roughness with application to contact mechanics, sealing, rubber friction and adhesion," Jan. 12, 2005. 10.1088/0953-8984/17/1/R01.
[56] Persson BNJ. Theory of rubber friction and contact mechanics. J Chem Phys Aug. 2001;115(8):3840–61. https://doi.org/10.1063/1.1388626.
[57] V. der, B. Lorenz, and U.-P. rer nat Stefan Blügel, *Contact mechanics and friction of elastic solids on hard and rough substrates*. 2012. [Online]. Available: http://www.fz-juelich.de/zb.
[58] Ding S, Wang KCP, Yang E, Zhan Y. Influence of effective texture depth on pavement friction based on 3D texture area. Constr Build Mater Jun. 2021;287. https://doi.org/10.1016/j.conbuildmat.2021.123002.
[59] L. Goubert and U. Sandberg, "Enveloping texture profiles for better modelling of the rolling resistance and acoustic qualities of road pavements," 2017. [Online]. Available: www.rosanneproject.eu.
[60] Guo W, Chu L, Yang L, Fwa TF. Determination of tire rubber-pavement directional coefficient of friction based on contact mechanism considerations. Tribol Int Jan. 2023;179. https://doi.org/10.1016/j.triboint.2022.108178.
[61] Yang L, Chu L, Zhou B, Guo W, Fwa TF. Characterizing directional traffic-induced wear of road pavements. Wear Jan. 2022;488–489. https://doi.org/10.1016/j.wear.2021.204129.
[62] Clapp TG. Spectral correlation of the surface profile in the development of a tire and pavement interaction force model. Doctoral dissertation. North Carolina State University; 1983.
[63] P. Klein and J.-F. Hamet, "Road texture and rolling noise: an envelopment procedure for tire-road contact," 2004. [Online]. Available: https://hal.science/hal-00546120v1.
[64] Von Meier A, Van Blokland GJ, Descornet G. The influence of texture and sound absorption on the noise of porous road surfaces. In: Second International Symposium on Road Surface Characteristics; 1992. p. 7–19.
[65] Matuško J, Petrović I, Perić N. Neural network based tire/road friction force estimation. Eng Appl Artif Intell Apr. 2008;21(3):442–56. https://doi.org/10.1016/j.engappai.2007.05.001.
[66] G. Biau and G.B. Fr, "Analysis of a random forests model," 2012.
[67] Taghavifar H, Mardani A, Karim-Maslak H, Kalbkhani H. Artificial Neural Network estimation of wheel rolling resistance in clay loam soil. Appl Soft Comput J 2013;13(8):3544–51. https://doi.org/10.1016/j.asoc.2013.03.017.
[68] Farhadi P, Golmohammadi A, Sharifi A, Shahgholi G. Prediction of the tractor tire contact area, contact volume and rolling resistance using regression model and artificial neural network. Agric Eng Int: CIGR J 2019;21(3) [Online]. Available, http://www.cigrjournal.org.
[69] Olazagoitia JL, Perez JA, Badea F. Identification of tire model parameters with artificial neural networks. Appl Sci (Switz) Dec. 2020;10(24):1–16. https://doi.org/10.3390/app10249110.
[70] Cano-Ortiz S, Pascual-Muñoz P, Castro-Fresno D. Machine learning algorithms for monitoring pavement performance. Elsevier B.V.; 2022. https://doi.org/10.1016/j.autcon.2022.104309.
[71] Donavan PR. Use of the ASTM Standard Reference Test Tire as a benchmark for on-board tire/pavement noise measurement. *SAE technical paper*, no. 2009-01–2108. 2009.
[72] Ejsmont JA, Ronowski G, Świeczko-Żurek B, Sommer S. Road texture influence on tyre rolling resistance. Road Mater Pavement Des Jan. 2017;18(1):181–98. https://doi.org/10.1080/14680629.2016.1160835.
[73] Srirangam Santosh K, Anupam Kumar, Kasbergen Cor, Scarpas Athanasios, Cerezo Veronique. Study of influence of operating parameters on braking friction and rolling resistance. Transp Res Rec Jan. 2015;2525(1):79–90. https://doi.org/10.3141/2525-09.
[74] Rijkswaterstaat, "Wegenoverzicht - informatie en data," Rijkswaterstaat.
[75] S. Erkens, A. Varveri, W. Verwaal, and van de Ven, Martin, "Synthesis report on the composition and quality of ZOAB," 2019.
[76] Schönberger JL, Zheng E, Frahm JM, Pollefeys M. Pixelwise view selection for unstructured multi-view stereo. Lecture notes in computer science (including subseries lecture notes in artificial intelligence and lecture notes in bioinformatics). Springer Verlag; 2016. p. 501–18. https://doi.org/10.1007/978-3-319-46487-9_31.
[77] J.L. Schönberger and J.-M. Frahm, "Structure-from-motion revisited," 2016. [Online]. Available: https://github.com/colmap/colmap.
[78] J.L. Schönberger, T. Price, T. Sattler, J.-M. Frahm, and M. Pollefeys, "A vote-and-verify strategy for fast spatial verification in image retrieval," 2017. [Online]. Available: https://github.com/vote-and-verify.
[79] Blender Documentation Team, "Blender 4.3 Reference manual." Accessed: Jan. 27, 2025. [Online]. Available: https://docs.blender.org/manual/en/latest/copyright.html.
[80] W.L.C. Van Aalst, G.B. Derksen, P.P.M. Schackmann, F.G.M. Bouman, and; P. Paffen, "Automated ravelling inspection and maintenance planning on porous asphalt in the Netherlands," 2015. [Online]. Available: www.ndt.net/?id=18348.
[81] J. Laurent, J.F. Hébert, and M. Talbot, "Using full lane 3D road texture data for the automated detection of sealed cracks, bleeding and ravelling," 2017.
[82] M. Haider, M. Conter, O. Boujard, J.A. Ejsmont, T. Wang, and J.T. Harvey, "Rolling resistance – Basic information and State-of the-art on measurement methods," 2011. [Online]. Available: http://www.miriam-co2.net/.
[83] De Graaff D.F., Hooghwerff J., van Gils E.W., and Reinink H.F., "Influence of road surface type on rolling resistance: rolling resistance measurement programme 2012," 2012.
[84] Smith M., "Abaqus/CAE User's Manual Abaqus 6.11 Abaqus/CAE, User's Manual," 2009.
[85] Namjoo M, Golbakhshi H. An efficient design tool based on FEM for evaluating effects of components properties and operating conditions on interaction of tire with rigid road. J Cent South Univ Jan. 2015;22(1):189–95. https://doi.org/10.1007/s11771-015-2509-7.
[86] Srirangam SK, Anupam K, Scarpas A, Kösters A. Influence of tire temperature increase on friction measurements-I: laboratory tests and finite element modeling aspects. In: Proceedings of the Transportation Research Board Annual Meeting; 2013. p. 13–7.
[87] Premarathna WAAS, Jayasinghe JASC, Wijesundara KK, Gamage P, Ranatunga RRMSK, Senanayake CD. Investigation of design and performance improvements on solid resilient tires through numerical simulation. Eng Fail Anal Oct. 2021;128. https://doi.org/10.1016/j.engfailanal.2021.105618.
[88] Tang T, Anupam K, Kasbergen C, Kogbara R, Scarpas A, Masad E. Finite element studies of skid resistance under hot weather condition. Transp Res Rec Dec. 2018;2672(40):382–94. https://doi.org/10.1177/0361198118796728.
[89] Srirangam SK, Anupam K, Scarpas A, Kasbergen C. Development of a thermomechanical tyre–pavement interaction model. Int J Pavement Eng Sep. 2015;16(8):721–9. https://doi.org/10.1080/10298436.2014.946927.
[90] Anupam K, Tang T, Kasbergen C, Scarpas A, Erkens S. 3-D thermomechanical tire–Pavement interaction model for evaluation of pavement skid resistance. Transp Res Rec Mar. 2021;2675(3):65–80. https://doi.org/10.1177/0361198120963101.
[91] Yang P, Zang M, Zeng H, Guo X. The interactions between an off-road tire and granular terrain: gPU-based DEM-FEM simulation and experimental validation. Int J Mech Sci 2020;179:105634.
[92] Ge Y, Yan Y, Yan X, Meng Z. Extending the tire dynamic model range of operating conditions based on finite element method. Adv Mech Eng Mar. 2022;14(3). https://doi.org/10.1177/16878132221085454.
[93] Ahmad F, Khan RA. A power comparison of various normality tests. Pak J Stat Oper Res 2015:331–45.
[94] D. Luo, X. Wan, J. Liu, and T. Tong, "Testing normality using the summary statistics with application to meta-analysis," *arXiv preprint arXiv:1801.09456*, 2018.
[95] DeWees TA, Mazza GL, Golafshar MA, Dueck AC. Investigation into the effects of using normal distribution theory methodology for Likert scale patient-reported outcome data from varying underlying distributions including floor/ceiling effects. Value Health 2020;23(5):625–31. https://doi.org/10.1016/j.jval.2020.01.007.
[96] Khatun N, others. Applications of normality test in statistical analysis. Open J Stat 2021;11(01):113.
[97] Rosner B, Glynn RJ, Lee M-LT. The Wilcoxon signed rank test for paired comparisons of clustered data. Biometrics 2006;62(1):185–92.
[98] Shieh G, Jan S-L, Randles RH. Power and sample size determinations for the Wilcoxon signed-rank test. J Stat Comput Simul 2007;77(8):717–24.
[99] Durango A, Refugio C. An empirical study on Wilcoxon signed rank test. J Negros Orient State Univ(Dec) 2018.